View metadata, citation and similar papers at core.ac.uk

brought to you by CORE

provided by Repositorio Institucional de la Universidad de Alicante

Accepted Manuscript

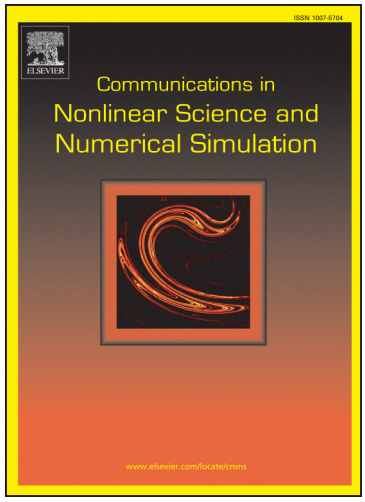

Steady-state, self-oscillating and chaotic behavior of a PID controlled nonlinear servomechanism by using Bogdanov-Takens and Andronov-Poincaré-Hopf bifurcations

Manuel Pérez-Molina, Manuel F.Pérez-Polo

PII: S1007-5704(14)00103-8
DOI: http://dx.doi.org/10.1016/j.cnsns.2014.03.003
Reference: CNSNS 3123

To appear in: *Communications in Nonlinear Science and Numerical Simulation*

Received Date: 11 May 2013
Revised Date: 3 March 2014
Accepted Date: 3 March 2014

Please cite this article as: Pérez-Molina, M., F.Pérez-Polo, M., Steady-state, self-oscillating and chaotic behavior of a PID controlled nonlinear servomechanism by using Bogdanov-Takens and Andronov-Poincaré-Hopf bifurcations, *Communications in Nonlinear Science and Numerical Simulation* (2014), doi: http://dx.doi.org/10.1016/j.cnsns.2014.03.003

This is a PDF file of an unedited manuscript that has been accepted for publication. As a service to our customers we are providing this early version of the manuscript. The manuscript will undergo copyediting, typesetting, and review of the resulting proof before it is published in its final form. Please note that during the production process errors may be discovered which could affect the content, and all legal disclaimers that apply to the journal pertain.

ACCEPTED MANUSCRIPT

Steady-state, self-oscillating and chaotic behavior of a PID controlled nonlinear servomechanism by using Bogdanov-Takens and Andronov-Poincaré-Hopf bifurcations

Manuel Pérez-Molina[a], Manuel F.Pérez-Polo[b*]

Departamento de Física, Ingeniería de Sistemas y Teoría de la Señal, Universidad de Alicante, Escuela Politécnica Superior, Campus de San Vicente, 03071, Alicante, Spain. Fax 34 965909750, Tel: 34 965909673. E-mail: [a]E-mail: ma_perez_m@hotmail.com. [b*]manolo@dfists.ua.es,

Abstract

This paper analyzes a controlled servomechanism with feedback and a cubic nonlinearity by means of the Bogdanov-Takens and Andronov-Poincaré-Hopf bifurcations, from which steady-state, self-oscillating and chaotic behaviors will be investigated using the center manifold theorem. The system controller is formed by a Proportional plus Integral plus Derivative action (PID) that allows to stabilize and drive to a prescribed set point a body connected to the shaft of a DC motor. The Bogdanov-Takens bifurcation is analyzed through the second Lyapunov stability method and the harmonic-balance method, whereas the first Lyapunov value is used for the Andronov-Poincaré-Hopf bifurcation. On the basis of the results deduced from the bifurcation analysis, we show a procedure to select the parameters of the PID controller so that an arbitrary steady-state position of the servomechanism can be reached even in presence of noise. We also show how chaotic behavior can be obtained by applying a harmonical external torque to the device in self-oscillating regime. The advantage of achieving chaotic behavior is that it can be used so that the system reaches a set point inside a strange attractor with a small control effort. The analytical calculations have been verified through detailed numerical simulations.

Keywords: Servomechanism, Bogdanov-Takens bifurcation, Andronov-Poincaré-Hopf bifurcation, center manifold, chaotic behavior, PID controller.

b* Author whose correspondence should be addressed

ACCEPTED MANUSCRIPT

1. Introduction

The study of electromechanical devices has focused almost entirely on linear systems, although nowadays it is widely recognized that an analysis based on linear models can be inadequate for devices with strong nonlinearities and for sufficiently large excursions from the equilibrium point [1-3]. On the other hand, the bifurcation theory has not been widely used in the analysis of the multidimensional controlled electromechanical systems. For example, the Bogdanov-Takens (BT) bifurcation (i.e. when the matrix of the linear part of the system has two null eigenvalues) [4-12] or the Andronov-Poincaré-Hopf (APH) bifurcation (which appears if the matrix of the linear part of the system has two pure imaginary eigenvalues) [13-20] has not been of common use in the resolution of problems associated to nonlinear oscillations in complex systems.

This paper considers the motion of a servomechanism, whose mathematical model includes a potentiometer, a PID controller, a cubic nonlinearity, an amplifier, and a DC motor with a gear train controlled by armature, which provides a nonlinear feedback control system. It is assumed that an external disturbance torque formed by a constant term plus a harmonic one is applied to the output axis of the servomechanism. The present paper has two main purposes. The first one is to design the PID controller so that the output shaft of the servomechanism can reach a prescribed set point, which will be achieved on the basis of the results obtained from a detailed analysis of the BT and APH bifurcations. The second goal of the paper is to use the aforementioned bifurcation analysis to obtain chaotic behavior, which will be advantageously used to reach a predetermined set point with a small control effort, even in the presence of noise.

The paper is organized as follows. In section 3, the BT bifurcation is analyzed by applying the center manifold theorem, which allows obtaining the normal form of the system, i.e. the simplest form of the system in R^2 which contains all the dynamics properties of the original system -defined in R^4-. In section 4, the stability of the normal form of the system is studied from the Lyapunov's direct method by means of a candidate Lyapunov function [1]. Consequently, the proportional constant and the reset time of a PID controller can be tuned to find out the stability of a predefined set point or

ACCEPTED MANUSCRIPT

to predict a self-oscillating behavior. The previous procedure does not provide the derivative control action of the PID, which has been determined through the harmonic balance method (describing function) [1], [21-22]. In addition, the self-oscillation frequency has also been obtained in section 4.

In section 5, the servomechanism is analyzed from a computational viewpoint. The purpose is to demonstrate how the self-oscillation regime can be predicted from the parameters of the PID controller deduced in section 4, and how the chaotic behavior can appear. Once the self-oscillating regime has been reached with the BT bifurcation, it is demonstrated that the harmonic variation of the reference input can give rise to chaotic dynamics, which has been investigated from the analysis of the sensitive dependence, Lyapunov exponents, power spectral density, Poincaré sections and bifurcation diagrams. Consequently, a new family of strange attractors has been characterized. It should be noticed that, in systems from which experimental data can be obtained, the methods of nonlinear time series [23] can also be used to corroborate whether an attractor is chaotic or not.

In section 6, the APH bifurcation is analyzed, and it is demonstrated that it can only appear if the external disturbance torque in the motor shaft has a non null mean value (which arises from a constant term). In this case, the self-oscillating conditions and the oscillation frequency are deduced by applying the Routh stability criteria to the linearized system at the equilibrium point. Consequently, the parameters of the PID controller can be designed to obtain an equilibrium point that is a weak focus [23], whose stability will be analyzed from the calculation of the first Lyapunov value [13-18], [24-25] (since the analytical calculations are very cumbersome, a computational procedure to obtain the first Lyapunov value has been included in an Appendix). The simulation results shows that an unstable weak focus (i.e. a positive value of the first Lyapunov value) results in an unstable system.

Once the self-oscillating behavior due to an APH bifurcation has been reached, as in the case of BT bifurcation, chaotic dynamics can appear when an external harmonic disturbance is applied, so a new family of chaotic attractors has been obtained, which can be used to reach the set point with small control signals. It is

ACCEPTED MANUSCRIPT

interesting to point out that the partial control method [26-28] represents an alternative procedure for using the chaotic behavior to maintain the system in a small zone of the phase plane employing small control signals even in presence of noise.

2. Mathematical model

The system is formed by a body to be stabilized that is driven by a gear train (regarded as ideal) with a transmission relation $n = N_1/N_2$. The gear train is connected to a DC field-controlled motor to which an input voltage $u_a(t)$ is applied through an amplifier with constant K_a [2]. The feedback is carried out by means of a potentiometer with constant K_s, whose output voltage u(t) is applied to a PID controller connected to a nonlinear cubic element with a constant K_{ne} as shown in Fig 1.

The nomenclature and parameter values of the subsystems which form the servomechanism (i.e.: potentiometer, PID controller, nonlinear element, amplifier and DC motor with a gear train) are shown in Table 1. The rest of parameters associated to the analysis of the BT and APH bifurcations, stability by means of Lyapunov's direct method, describing function and calculation of the first Lyapunov value are defined in each section, subsection and in the Appendix.

Figure 1

Table 1

This device can be applied for tracking mechanical systems such as image tracking systems, in which a nonlinear element with zero-sensitivity zone type that can be approximated by a cubic parabola [29-30]. The mathematical equations of the system are the following ones:

- Potentiometer equation:

$$u(t) = K_s\left[\theta_r(t) - \theta(t)\right] \tag{1}$$

- PID controller equation:

$$u_1(t) = K_p\left[u(t) + \frac{1}{\tau_i}\int_0^t u(\sigma)\,d\sigma + \tau_d\frac{du(t)}{dt}\right] \tag{2}$$

ACCEPTED MANUSCRIPT

where K_p, is the proportional constant, τ_i is the reset time and τ_d is the derivative time [31-33].

- Equation of the nonlinear element:

$$u_2(t) = K_{ne} u_1^3(t) \tag{3}$$

- Amplifier equation:

$$u_a(t) = K_a u_2(t) \tag{4}$$

- Equation of the armature current:

$$\begin{aligned} L_a \frac{di_a(t)}{dt} + R_a i_a(t) &= u_a(t) - u_b(t) \\ u_b(t) = K_b \omega_m(t) &= K_b \frac{d\theta_m(t)}{dt} \end{aligned} \tag{5}$$

where $u_b(t)$ is the back-electromotive force, $\theta_m(t)$ is the angle of the motor shaft and $\omega_m(t)$ is the angular velocity of the motor shaft.

- Equation of the motor torque:

$$\begin{aligned} J_{me} \frac{d^2\theta_m(t)}{dt^2} + B_{me} \frac{d\theta_m(t)}{dt} &= T_m(t) \;\; ; \;\; J_{me} = J_m + \left(N_1/N_2\right)^2 J_L \\ B_{me} = B_m + \left(N_1/N_2\right)^2 B_L \;\; ; \;\; T_m(t) &= T_m'(t) + T_L'(t) + T_d(t) \end{aligned} \tag{6}$$

where J_m and J_L are the inertia moments of the motor shaft and load respectively, B_m and B_L are the viscous friction of the motor and load, and J_{me} and B_{me} are the equivalent inertia moment and viscous friction, both of them with respect to the motor shaft. On the other hand, $T_m(t)$, $T'_m(t)$, $T'_L(t)$ and $T_d(t)$ are respectively the motor torque, the motor torque to move the shaft plus the motor viscous friction, the load torque and the disturbance torque.

- Motor torque assuming a linear regime:

ACCEPTED MANUSCRIPT

$$T_m(t) = K_m i_a(t) \tag{7}$$

where K_m is the torque constant.

The reference input $\theta_r(t)$ and the disturbance torque $T_d(t)$ are defined as:

$$\theta_r(t) = \theta_{r1} + \theta_{r2}\sin(\omega_r t) \;\; ; \;\; T_d(t) = T_{d1} + T_{d2}\sin(\omega_d t) \tag{8}$$

It should be noticed that it is possible to choose different input signals. For example, we have a step input for $\theta_{r2} = 0$, whereas the disturbance torque is constant for $T_{d2} = 0$.

The mathematical model of the device can be defined by two equivalent systems of equations; one of them is based on the output angle $\theta(t)$ of the axis and the other one is based on the input voltage of the PID controller u(t) (see Fig 1). Since $\theta_m = (N_2/N_1)\theta = \theta/n$, from Eqs (6) and (7) it is deduced that:

$$\frac{J_{me}}{n}\frac{d^3\theta(t)}{dt^3} + \frac{B_{me}}{n}\frac{d^2\theta(t)}{dt^2} = K_m\frac{di_a(t)}{dt} \tag{9}$$

$$\frac{di_a(t)}{dt} = -\frac{R_a}{L_a}i_a(t) + \frac{K_a}{L_a}u_2(t) - \frac{K_b}{nL_a}\frac{d\theta(t)}{dt} \tag{10}$$

Substituting Eq (10) into Eq (9) it is deduced that:

$$\frac{J_{me}}{n}\frac{d^3\theta(t)}{dt^3} + \frac{B_{me}}{n}\frac{d^2\theta(t)}{dt^2} + \frac{K_m K_b}{nL_a}\frac{d\theta(t)}{dt} = -\frac{K_m R_a}{L_a}i_a(t) + \frac{K_m K_a}{L_a}u_2(t) \tag{11}$$

On the other hand, the armature current $i_a(t)$ can be deduced from Eqs (6) and (7) as:

$$i_a(t) = \frac{J_{me}}{nK_m}\frac{d^2\theta(t)}{dt^2} + \frac{B_{me}}{nK_m}\frac{d\theta(t)}{dt} \tag{12}$$

In order to substitute Eq (12) into Eq (11) it is convenient to introduce the following nomenclature:

ACCEPTED MANUSCRIPT

$$\tau^2 = \frac{J_{me}L_a}{K_mK_b + R_aB_{me}} \;;\; K' = \frac{nK_mK_a}{J_{me}L_a}\tau^2 \;;\; 2\xi\tau = \left(\frac{B_{me}}{J_{me}} + \frac{R_a}{L_a}\right)\frac{J_{me}L_a}{K_mK_b + R_aB_{me}} \;;\; K = K_{ne}K_sK'$$

$$\xi = \frac{1}{2}\left(\frac{B_{me}}{J_{me}} + \frac{R_a}{L_a}\right)\sqrt{\frac{J_{me}L_a}{K_mK_b + R_aB_{me}}} \;;\; K_m = \sqrt{\frac{L_aJ_{me}}{4\xi^2}\left[\left(\frac{B_{me}}{J_{me}}\right) + \left(\frac{R_a}{L_a}\right)\right] - R_aB_{me}}$$

(13)

where K_m is calculated as a function of ξ. It can be verified that ξ is a dimensionless parameter, whereas the units of τ, K' and K are seconds (s), $V^{-1}s^{-1}$ and $V^{-2}s^{-1}$ respectively. From Eqs (8)-(13) it is possible to determine a differential equation in terms of the θ(t), in which u(t) as well as the integral action in the PID controller can be eliminated between Eqs (1) and (2). Thus the mathematical model of the system can be written as follows:

$$\frac{d^3\theta(t)}{dt^3} + \frac{2\xi}{\tau}\frac{d^2\theta(t)}{dt^2} + \frac{1}{\tau^2}\frac{d\theta(t)}{dt} = \frac{K'K_{ne}}{\tau^2}u_1^3(t) - \frac{n}{J_{me}}\frac{R_a}{L_a}T_d(t) - \frac{n}{J_{me}}\frac{dT_d(t)}{dt}$$

$$\frac{du_1(t)}{dt} = -\frac{K_pK_s}{\tau_i}\theta(t) - K_pK_s\frac{d\theta(t)}{dt} - K_pK_s\tau_d\frac{d^2\theta(t)}{dt^2} + \frac{K_pK_s}{\tau_i}\theta_r(t) + \quad (14)$$

$$+ K_pK_s\frac{d\theta_r(t)}{dt} + K_pK_s\tau_d\frac{d^2\theta_r(t)}{dt^2}$$

Taking into account Eq (1), it is possible to deduce an equivalent mathematical model expressed as a function of u(t), so from Eqs (1) and (14) it is deduced that:

$$\frac{d^3u(t)}{dt^3} + \frac{2\xi}{\tau}\frac{d^2u(t)}{dt^2} + \frac{1}{\tau^2}\frac{du(t)}{dt} = -\frac{K}{\tau^2}u_1^3(t) + \frac{nK_s}{J_{me}}\frac{R_a}{L_a}T_d(t) + \frac{nK_s}{J_{me}}\frac{dT_d(t)}{dt}$$

$$+ K_s\frac{d^3\theta_r(t)}{dt^3} + \frac{2\xi K_s}{\tau}\frac{d^2\theta_r(t)}{dt^2} + \frac{K_s}{\tau^2}\frac{d\theta_r(t)}{dt} \quad (15)$$

$$\frac{du_1(t)}{dt} = \frac{K_p}{\tau_i}u(t) + K_p\frac{du(t)}{dt} + K_p\tau_d\frac{d^2u(t)}{dt^2}$$

Eqs (8), (14) and (15) will be used in the analysis of the BT [4-12] and APH bifurcations [13-20]. It is interesting to remark that the relation θ(t) = θ(t) + 2πk (k = 0, ±1, ±2,..) must be taken into account in the numerical integration of Eqs (14), whereas Eqs (15) can be directly solved using the appropriate initial conditions. In accordance

ACCEPTED MANUSCRIPT

with Eqs (13), Fig 2 shows the variation of the constant motor K_m, the time constant τ and the parameter K as function of ξ and R_a/L_a. It is clear that small values for ξ can be inappropriate to obtain an admissible value for K_m.

Figure 2

3. Analysis of the Bogdanov-Takens bifurcation

The BT bifurcation is analyzed from Eqs (15), for which we first assume that there is no disturbance torque (i.e. $T_d(t) \equiv 0$) and that the reference input is a step function of value θ_{r1} ($\theta_{r2} = 0$). The effect of θ_{r2} and T_{d2} will be examined later in the analysis of the chaotic behavior. Introducing the state variables:

$$x_1(t) = u(t) \;\; ; \;\; x_2(t) = \frac{du(t)}{dt} \;\; ; \;\; x_3(t) = \frac{d^2u(t)}{dt^2} \;\; ; \;\; x_4(t) = u_1(t) \tag{16}$$

Eqs (15) can be rewritten as follows:

$$\dot{x}(t) = Ax(t) + Bx_4^3(t) \Rightarrow \begin{bmatrix} \dot{x}_1(t) \\ \dot{x}_2(t) \\ \dot{x}_3(t) \\ \dot{x}_4(t) \end{bmatrix} = \begin{bmatrix} 0 & 1 & 0 & 0 \\ 0 & 0 & 1 & 0 \\ 0 & -1/\tau^2 & -2\xi/\tau & 0 \\ K_p/\tau_i & K_p & K_p\tau_d & 0 \end{bmatrix} \begin{bmatrix} x_1(t) \\ x_2(t) \\ x_3(t) \\ x_4(t) \end{bmatrix} + \begin{bmatrix} 0 \\ 0 \\ -K/\tau^2 \\ 0 \end{bmatrix} x_4^3(t) \tag{17}$$

It can be verified that the eigenvalues of matrix A are given by:

$$\begin{gathered} |\lambda I - A| = \lambda^2 \left[\lambda^2 + (2\xi/\tau)\lambda + (1/\tau^2) \right] = 0 \\ \lambda_{1,2} = 0 \;\; ; \;\; \lambda_{3,4} = -\alpha \pm \omega j \;\; ; \;\; \alpha = \xi/\tau \;\; ; \;\; \omega = \sqrt{1-\xi^2}/\tau \;\; ; \;\; \text{for} \;\; 0 < \xi < 1 \\ \lambda_{1,2} = 0 \;\; ; \;\; \lambda_{3,4} = -\alpha_{1,2} \;\; ; \;\; \alpha_{1,2} = \xi/\tau \pm \sqrt{\xi^2 - 1}/\tau \;\; ; \;\; \text{for} \;\; \xi \geq 1 \end{gathered} \tag{18}$$

Consequently, a double zero eigenvalue appears (Bogdanov-Takens bifurcation) in the equilibrium point of Eqs (17), which is the origin. The analysis of this bifurcation will be carried out through a series of steps to obtain a simplified system reduced to the center manifold [5-12]:

ACCEPTED MANUSCRIPT

It should be remarked that the BT bifurcation is due to the fact that the disturbance torque is zero, i.e. $T_d(t) \equiv 0$. If the disturbance torque is a nonzero constant, i.e. $T_d(t) = T_{d1} \neq 0$, the origin is not an equilibrium point. Consequently, by introducing the deviation variable $x_4'(t) = x_4(t) - x_{4e}$ to move the equilibrium point to the origin, Eqs (17) allow to deduce that the term *A(3,4)* of the new matrix *A* is not zero. Thus the eigenvalues $\lambda_{1,2}$ are now different of zero, so the BT bifurcation disappears.

- Step 1:

We shall denote by P_1 the matrix that transforms the linear part of Eq (11) into its Jordan canonical form when it has two complex conjugate eigenvalues ($0<\xi<1$), whereas P_2 shall denote the same matrix in case the four eigenvalues are real ($\xi \geq 1$). Then the columns of P_1 and P_2 are the eigenvectors associated to the eigenvalues of Eq (18), so it follows that:

For $0 < \xi < 1$:

$$x = P_1 \bar{x} \Rightarrow \begin{bmatrix} x_1 \\ x_2 \\ x_3 \\ x_4 \end{bmatrix} = \begin{bmatrix} 0 & \tau_i / K_p & 0 & 1 \\ 0 & 0 & \omega & -\alpha \\ 0 & 0 & -2\alpha\omega & \alpha^2 - \omega^2 \\ 1 & 0 & b_1 & a_1 \end{bmatrix} \begin{bmatrix} x \\ y \\ z \\ w \end{bmatrix} \quad \begin{cases} a_1 = \dfrac{-\alpha K_p / \tau_i}{\alpha^2 + \omega^2} + K_p (1 - \tau_d \alpha) \\ b_1 = \dfrac{-\omega K_p / \tau_i}{\alpha^2 + \omega^2} + K_p \tau_d \omega \end{cases}$$

For $\xi \geq 1$:

$$x = P_2 \bar{x} \Rightarrow \begin{bmatrix} x_1 \\ x_2 \\ x_3 \\ x_4 \end{bmatrix} = \begin{bmatrix} 0 & \tau_i / K_p & 1 & 1 \\ 0 & 0 & \alpha_1 & \alpha_2 \\ 0 & 0 & \alpha_1^2 & \alpha_2^2 \\ 1 & 0 & b_2 & a_2 \end{bmatrix} \begin{bmatrix} x \\ y \\ z \\ w \end{bmatrix} \quad \begin{cases} a_2 = K_p + K_p \tau_d \alpha_2 + \dfrac{K_p}{\alpha_2 \tau_i} \\ b_2 = K_p + K_p \tau_d \alpha_1 + \dfrac{K_p}{\alpha_1 \tau_i} \end{cases}$$

(19)

- Step 2

From the new coordinates given by Eq (19), the system (17) can be rewritten in the canonical Jordan form as follows:

ACCEPTED MANUSCRIPT

For $0<\xi<1$:

$$\begin{bmatrix}\dot{x}\\ \dot{y}\\ \dot{z}\\ \dot{w}\end{bmatrix}=\begin{bmatrix}0 & 1 & 0 & 0\\ 0 & 0 & 0 & 0\\ 0 & 0 & -\alpha & -\omega\\ 0 & 0 & \omega & -\alpha\end{bmatrix}\begin{bmatrix}x\\ y\\ z\\ w\end{bmatrix}+P_1^{-1}\begin{bmatrix}0\\ 0\\ -K/\tau^2\\ 0\end{bmatrix}\left(x+b_1z+a_1w\right)^3$$

For $\xi\geq 1$:

$$\begin{bmatrix}\dot{x}\\ \dot{y}\\ \dot{z}\\ \dot{w}\end{bmatrix}=\begin{bmatrix}0 & 1 & 0 & 0\\ 0 & 0 & 0 & 0\\ 0 & 0 & -\alpha_1 & 0\\ 0 & 0 & 0 & -\alpha_2\end{bmatrix}\begin{bmatrix}x\\ y\\ z\\ w\end{bmatrix}+P_2^{-1}\begin{bmatrix}0\\ 0\\ -K/\tau^2\\ 0\end{bmatrix}\left(x+b_2z+a_2w\right)^3 \quad (20)$$

where P_1^{-1} and P_2^{-1} are the inverse matrices of P_1 and P_2 respectively. On the other hand we have that:

For $0<\xi<1$:

$$P_1^{-1}\begin{bmatrix}0\\ 0\\ -K/\tau^2\\ 0\end{bmatrix}=\frac{1}{\Delta_1}\begin{bmatrix}0 & p_{112}^{-1} & p_{113}^{-1} & \Delta_1\\ \omega\left(\alpha^2+\omega^2\right) & 2\alpha\omega & \omega & 0\\ 0 & -\left(\tau_i/K_p\right)\left(\alpha^2-\omega^2\right)/\omega & -\tau_i\alpha/K_p & 0\\ 0 & -2\tau_i\alpha\omega/K_p & -\tau_i\omega/K_p & 0\end{bmatrix}\begin{bmatrix}0\\ 0\\ -K/\tau^2\\ 0\end{bmatrix}$$

$$\Delta_1=\frac{K_p}{\tau_i\omega\left(\alpha^2+\omega^2\right)}\ ;\ p_{112}^{-1}=\frac{\tau_i}{K_p}\left[2\alpha\omega a_1+b_1\left(\alpha^2-\omega^2\right)\right]\ ;\ p_{113}^{-1}=\frac{\tau_i}{K_p}\left(\omega a_1+\alpha b_1\right)$$

For $\xi\geq 1$:

$$P_2^{-1}\begin{bmatrix}0\\ 0\\ -K/\tau^2\\ 0\end{bmatrix}=\frac{1}{\Delta_2}\begin{bmatrix}0 & p_{212}^{-1} & p_{213}^{-1} & \Delta_2\\ \alpha_1\alpha_2\left(\alpha_1-\alpha_2\right) & \alpha_2^2-\alpha_1^2 & \alpha_2-\alpha_1 & 0\\ 0 & -\tau_i\alpha_2^2/K_p & -\tau_i\alpha_2/K_p & 0\\ 0 & \tau_i\alpha_1^2/K_p & \tau_i\alpha_1/K_p & 0\end{bmatrix}\begin{bmatrix}0\\ 0\\ -K/\tau^2\\ 0\end{bmatrix}$$

$$\Delta_2=\frac{1}{\left(\tau_i/K_p\right)\alpha_1\alpha_2\left(\alpha_1-\alpha_2\right)}\ ;\ p_{212}^{-1}=\frac{\tau_i}{K_p}\left(\alpha_2^2b_2-\alpha_1^2a_2\right)\ ;\ p_{213}^{-1}=\frac{\tau_i}{K_p}\left(\alpha_2b_2-\alpha_1a_2\right)$$

(21)

where Δ_1 and Δ_2 are the determinants of the matrices P_1 and P_2 respectively. Taking into account Eq (21), Eq (20) can be rewritten as follows:

ACCEPTED MANUSCRIPT

For $0<\xi<1$:

$$\begin{bmatrix}\dot{x}\\ \dot{y}\\ \dot{z}\\ \dot{w}\end{bmatrix}=\begin{bmatrix}0 & 1 & 0 & 0\\ 0 & 0 & 0 & 0\\ 0 & 0 & -\alpha & -\omega\\ 0 & 0 & \omega & -\alpha\end{bmatrix}\begin{bmatrix}x\\ y\\ z\\ w\end{bmatrix}+\frac{K}{\omega}\begin{bmatrix}-\left(\omega a_1+\alpha b_1\right)\\ -K_p\omega/\tau_i\\ \alpha\\ \omega\end{bmatrix}\left(x+b_1z+a_1w\right)^3$$

For $\xi\geq 1$: (22)

$$\begin{bmatrix}\dot{x}\\ \dot{y}\\ \dot{z}\\ \dot{w}\end{bmatrix}=\begin{bmatrix}0 & 1 & 0 & 0\\ 0 & 0 & 0 & 0\\ 0 & 0 & -\alpha_1 & 0\\ 0 & 0 & 0 & -\alpha_2\end{bmatrix}\begin{bmatrix}x\\ y\\ z\\ w\end{bmatrix}+\left(\frac{-K}{\tau^2}\right)\begin{bmatrix}\dfrac{\alpha_1a_2-\alpha_2b_2}{\alpha_1\alpha_2\left(\alpha_1-\alpha_2\right)}\\ K_p/\alpha_1\alpha_2\tau_i\\ 1/\alpha_1\left(\alpha_1-\alpha_2\right)\\ -1/\alpha_2\left(\alpha_1-\alpha_2\right)\end{bmatrix}\left(x+b_2z+a_2w\right)^3$$

- Step 3

We now aim to simplify Eqs (22) as much as possible by using the center manifold theorem [14-16] to reduce the dimensionality to two in a neighborhood of the origin (equilibrium point). Since the nonlinearity is cubic, it is assumed that z and w are approximated by third-order polynomials, i.e.:

$$\left.\begin{aligned}z&=m_1x^3+m_2y^3+m_3x^2y+m_4xy^2\\ w&=n_1x^3+n_2y^3+n_3x^2y+n_4xy^2\end{aligned}\right\}\tag{23}$$

where m_i and n_i (i = *1,2,3,4*) are determined by applying the center manifold theorem. However, the coefficients n_i and m_i are not necessary to analyze the Bogdanov-Takens bifurcation, since the system reduced to the center manifold up to fifth-order terms (obtained by substituting Eqs (23) into Eqs (22)) can be written without involving such coefficients, i.e.:

For $0<\xi<1$:

$$\begin{bmatrix}\dot{x}\\ \dot{y}\end{bmatrix}=\begin{bmatrix}0 & 1\\ 0 & 0\end{bmatrix}\begin{bmatrix}x\\ y\end{bmatrix}+\frac{K}{\omega}\begin{bmatrix}-\left(\omega a_1+\alpha b_1\right)\\ -\dfrac{K_p\omega}{\tau_i}\end{bmatrix}x^3+\mathrm{O}\left(\|x\|^5\right)$$

For $\xi\geq 1$: (24)

$$\begin{bmatrix}\dot{x}\\ \dot{y}\end{bmatrix}=\begin{bmatrix}0 & 1\\ 0 & 0\end{bmatrix}\begin{bmatrix}x\\ y\end{bmatrix}+\frac{K}{\tau^2}\begin{bmatrix}-\dfrac{\alpha_1a_2-\alpha_2b_2}{\alpha_1\alpha_2\left(\alpha_1-\alpha_2\right)}\\ -K_p/\alpha_1\alpha_2\tau_i\end{bmatrix}x^3+\mathrm{O}\left(\|x\|^5\right)$$

ACCEPTED MANUSCRIPT

where $\mathrm{O}\left(\|x\|^5\right)$ accounts for fifth-order terms, which are neglected in a neighborhood of the origin. It should be noticed that the coefficients m_i and n_i (i = *1,2,3,4*) are only necessary if one wants to obtain the variables z(t) and w(t) from the variables x(t) and y(t) deduced from a third-order approximation of Eq (22). From Eqs (19), the initial variables of the system could be calculated and compared with the simulation results deduced from Eqs (17). On the other hand, from Eqs (19) and (24) it is deduced that:

$$\begin{aligned} d_1 &= -\frac{K}{\omega}\left(\omega a_1 + \alpha b_1\right) = -\frac{K}{\tau^2}\frac{\alpha_1 a_2 - \alpha_2 b_2}{\alpha_1\alpha_2\left(\alpha_1 - \alpha_2\right)} \\ d_2 &= -\frac{KK_p}{\tau_i} = -\frac{K}{\tau^2}\frac{K_p}{\alpha_1\alpha_2\tau_i} \end{aligned} \tag{25}$$

Eqs (25) allow to deduce that both conditions $0 < \xi < 1$ and $\xi \geq 1$ can be used for the stability analysis. For simplicity, we will only refer to the case $0 < \xi < 1$ taking into account that analogous results are obtained for $\xi \geq 1$. With the purpose of deducing the normal form of Eqs (24), we consider the following coordinate change:

$$\left.\begin{aligned} y &= \bar{y} - d_1\bar{x}^3 \\ x &= \bar{x} + \gamma\bar{x}^3 \end{aligned}\right\} \Rightarrow \left.\begin{aligned} \dot{y} &= \dot{\bar{y}} - 3d_1\bar{x}^2\dot{\bar{x}} \\ \dot{x} &= \dot{\bar{x}} + 3\gamma\bar{x}^2\dot{\bar{x}} \end{aligned}\right\} \tag{26}$$

where γ is a parameter that will be suitably chosen so that the system of Eqs (24) in the new variables $(\bar{x}, \bar{y})$ is simplified as much as possible. Substituting Eqs (26) into Eqs (24) and taking into account that only the terms up to the fifth order are necessary, Eqs (24) can be rewritten in the new variables as follows:

$$\begin{aligned} \dot{\bar{x}} &= \left(\bar{y} - d_1\bar{x}^3\right)\left(1 - 3\gamma\bar{x}^2\right) + d_1\left(\bar{x} + \gamma\bar{x}^3\right)^3\left(1 - 3\gamma\bar{x}^2\right) + \mathrm{O}\left(\|\bar{x}\|^5\right) \\ \dot{\bar{y}} &= 3d_1\bar{x}^2\dot{\bar{x}} + d_2\left(\bar{x} + \gamma\bar{x}^3\right)^3 + \mathrm{O}\left(\|\bar{x}\|^5\right) \end{aligned} \tag{27}$$

Taking $\gamma = 0$ in Eqs (27), the normal form of the BT bifurcation can be written in terms of the new variables $(\bar{x}, \bar{y})$ as follows:

ACCEPTED MANUSCRIPT

$$\begin{aligned}\dot{\bar{x}} &= \bar{y} + \mathrm{O}\left(\|\bar{x}\|^5\right) \\ \dot{\bar{y}} &= d_2\bar{x}^3 + 3d_1\bar{x}^2\dot{\bar{x}} + \mathrm{O}\left(\|\bar{x}\|^5\right)\end{aligned} \tag{28}$$

The system in Eq (28) has a double null eigenvalue and it preserves the invariance under the coordinate transformation $(\bar{x},\bar{y}) \to (-\bar{x},-\bar{y})$. It is interesting to remark that the parameters a_1 and b_1 in Eqs (19) are dimensionless; the parameters d_1 and d_2 defined in Eqs (28) have the units $V^{-2}s^{-1}$ and $V^{-2}s^{-2}$ respectively and the variables $(x,\bar{x})$ and $(y,\bar{y})$ have the units V and Vs^{-1} respectively.

It should be noticed that the inequality $\omega a_1 + \alpha b_1 > 0$ can be deduced directly from the arguments shown in pages 374 and 446 of Refs [14] and [16] respectively. However, the deduction of the previous inequality in this paper has been made from Eqs (29)-(32) in order to generalize the reasoning by introducing the dimensional parameter p and to obtain the period T_{os} of the self-oscillating behavior given by Eq (36). The parameter p and the period T_{os} will be used to corroborate the accurateness of the describing function in the next section.

4. Parameters of the PID controller deduced from the BT bifurcation and the describing function

In this section we shall analyze the BT bifurcation by determining the normal form as well as the conditions for self-oscillating and steady state behavior once the PID controller parameters have been specified. We shall demonstrate that the proportional constant K_p and the integral action τ_i can be obtained by applying the Lyapunov's direct method, whereas the derivative constant τ_d is specified by using the harmonic balance method (or describing function).

4.1 Procedure to determine admissible parameter values for the PID controller

ACCEPTED MANUSCRIPT

Once the system reduced to the center manifold has been obtained, the stability analysis of the system can be carried out by using the Lyapunov's method. For this purpose, we choose a tentative Lyapunov function given by:

$$V(\bar{x},\bar{y}) = \frac{1}{2} p\bar{x}^4 + \bar{y}^2 \tag{29}$$

where $p > 0$ is a dimensional parameter (with units $V^{-2}s^{-2}$) and $V(\bar{x},\bar{y})$ is a positive definite function. Taking the derivative with respect to the time in Eq (29) and substituting the truncated form in Eq (28) (i.e. neglecting fifth-order terms) it is deduced that:

$$\dot{V}(\bar{x},\bar{y}) = 2p\bar{x}^3\dot{\bar{x}} + 2\bar{y}\cdot\dot{\bar{y}} = 2(p+d_2)\bar{x}^3\bar{y} + 6d_1\bar{x}^2\bar{y}^2 \tag{30}$$

Taking into account Eqs (28) and (30) it is deduced that the origin will be asymptotically stable when $\dot{V}(\bar{x},\bar{y}) < 0$, which requires the following conditions:

$$p + d_2 = 0 \Rightarrow p - \frac{KK_p}{\tau_i} = 0 \;\; ; \;\; d_1 = -\frac{K}{\omega}(\omega a_1 + \alpha b_1) < 0 \Rightarrow (\omega a_1 + \alpha b_1) > 0 \tag{31}$$

Considering the substitution $K_p/\tau_i = p/K$ and taking into account Eqs (18) and (21) it is deduced that:

$$\omega a_1 + \alpha b_1 = K_p\omega - \frac{2\alpha\omega p}{K(\alpha^2+\omega^2)} \Rightarrow K_p > \frac{2\alpha p}{K(\alpha^2+\omega^2)} \;\; ; \;\; \tau_i = KK_p \tag{32}$$

It should be noticed that the derivative control action does not appear in Eq (32), and thus it cannot be determined from the analysis of the BT bifurcation. As a result of the previous analysis, the stability conditions are given by:

$$K_p > \frac{2\alpha p}{K(\alpha^2+\omega^2)} \Rightarrow K_p = \frac{2\alpha pf}{K(\alpha^2+\omega^2)} \;\; ; \;\; \tau_i = \frac{2\alpha pf}{\alpha^2+\omega^2} \tag{33}$$

ACCEPTED MANUSCRIPT

where the parameter $f \geq 1$ is introduced to calculate an admissible value for the proportional constant K_p. In accordance with Eqs (28), (31) and (33), for $f = 1$ it follows that:

$$\ddot{\bar{x}} = -p\bar{x}^3 \Rightarrow p\frac{\bar{x}^4}{2} + \bar{y}^2 = C \tag{34}$$

where C is an arbitrary constant. Consequently, a limit cycle appears in the phase plane of the system reduced to the center manifold and thus the condition for self-oscillating behavior has been obtained. Taking into account Eq (34), the period of the self-oscillation regime for the approximated system of Eq (28) can be deduced as follows:

$$\frac{d\bar{x}}{dt} = \sqrt{2}\sqrt{C - p\bar{x}^4/4} \Rightarrow t = \int_{\bar{x}_o}^{\bar{x}} \frac{d\bar{x}}{\sqrt{2}\sqrt{C - p\bar{x}^4/4}} \Rightarrow T_{os} = \frac{4}{\sqrt{2}}\int_{\bar{x}_o}^{0} \frac{d\bar{x}}{\sqrt{C - p\bar{x}^4/4}} \tag{35}$$

where $\bar{x}_0$ is an arbitrary initial condition and T_{os} is the period of the self-oscillation regime. Introducing the double change of variables given by $\left(p/4C\right)^{1/4}\bar{x} = y$ and $y = z^4$, Eq (35) can be rewritten in terms of the Beta function $B(q_1,q_2)$, i.e.:

$$T_{os} = \frac{2}{\bar{x}_0}\sqrt{\frac{8}{p}}\int_0^1 \frac{dy}{\sqrt{1-y^4}} = \frac{2}{\bar{x}_0}\sqrt{\frac{8}{p}}\left[\frac{1}{4}B\left(1/4,1/2\right)\right] \tag{36}$$

The importance of this self-oscillating behavior lies on the fact that, once it has been reached, the presence of a harmonic term in the input signal or an external harmonic disturbance in the load of the stabilization body can lead to chaotic oscillations in the device, as it will be analyzed in section 5. In the following subsection, the effect of parameter p is studied.

4.2 Determination of the derivative constant of the PID controller

In the analysis of the previous subsection, the derivative constant τ_d of the PID controller remained unknown. To overcome this problem, the harmonic balance technique or describing function [1], [21-22] shall be applied to investigate the influence of τ_d on the self-oscillating behavior. In view of Fig 1, and assuming a

ACCEPTED MANUSCRIPT

sinusoidal input signal $u_1(t) = U_{1m} \sin \omega t$ in the nonlinear element, the output voltage will be given by:

$$u_2(t) = K_{ne} u_1^3(t) = \frac{K_{ne} U_{1m}^3}{4} (3\sin \omega t - \sin 3\omega t) \tag{37}$$

On the other hand, taking the Laplace transform of the input and output signals of the PID controller as well as the input signals to the potentiometer and amplifier, the transfer functions of the PID controller and the system are the following ones:

$$G_{PID}(s) = \frac{U_1(s)}{U(s)} = K_p \left(1 + \frac{1}{\tau_i s} + \tau_d s\right) \;;\; G(s) = \frac{\theta(s)}{U_2(s)} = \frac{K'}{s\left(\tau^2 s^2 + 2\xi\tau s + 1\right)} \tag{38}$$

where "s" denotes the complex variable associated to the Laplace transform. Assuming that G(s) is a low-pass filter, the influence of the third harmonic can be regarded as negligible and therefore Eq (37) allows to deduce that:

$$u_2(t) \approx \frac{3K_{ne} U_{1m}^3}{4} \sin \omega t \Rightarrow u_2(t) \approx N(U_{1m}) \sin \omega t \Rightarrow N(U_{1m}) = \frac{3K_{ne} U_{1m}^3}{4} \tag{39}$$

Taking into account Eqs (38) and (39), the output of the transfer function G(s) will be:

$$\theta(t) = \frac{3K_{ne} U_{1m}^3}{4} \left|G(j\omega)\right| \sin\left(\omega t + \varphi_{1\theta}\right) \begin{cases} \left|G(j\omega)\right| = \dfrac{K'}{\omega\Delta} \sqrt{4\xi^2\tau^2\omega^2 + \left(1 - \tau^2\omega^2\right)^2} \\ \Delta = 4\xi^2\tau^2\omega^2 + \left(1 - \tau^2\omega^2\right)^2 \\ \varphi_{1\theta} = arctg\left(\dfrac{1 - \tau^2\omega^2}{2\xi\tau\omega}\right) \end{cases} \tag{40}$$

where $\left|G(j\omega)\right|$ is the modulus of $G(s)\big|_{s=j\omega}$ and $\varphi_{1\theta}$ is its argument. Taking into account Eqs (39) and (40), the output of the PID controller can be written as follows (see Fig 1):

ACCEPTED MANUSCRIPT

$$u_1(t) = \frac{3K_{ne}K_sU_{1m}^3}{4}\left|G(j\omega)\right|\sin\left(\omega t + \varphi_{1\theta} + \varphi_{1PID} + \pi\right)$$
$$\varphi_{1PID} = -arctg\left(\frac{1-\tau_i\tau_d\omega^2}{\tau_i\omega}\right) \tag{41}$$

Since $u_1(t)$ is known, by identifying the amplitude and phase in Eqs (39)-(41) it is deduced that:

$$\frac{3K_{ne}K_sU_{1m}^3}{4}\left|G(j\omega)\right| = U_{1m} \;\; ; \;\; \varphi_{1\theta} + \varphi_{1PID} + \pi = 0 \Rightarrow tg\left(\varphi_{1\theta} + \varphi_{1PID}\right) = 0$$
$$U_{1m} = \frac{2}{\sqrt{3K_{ne}K_s\left|G(j\omega)\right|}} \;\; ; \;\; \omega_{os} = \sqrt{\frac{\tau_i - 2\xi\tau}{\tau_i\tau\left(\tau - 2\xi\tau_d\right)}} \tag{42}$$

where U_{1m} and ω_{os} are respectively the input voltage in the nonlinear element and the self-oscillation frequency. From Eqs (42) it follows that:

$$\tau_i > 2\xi\tau \;;\; \tau > 2\xi\tau_d \Rightarrow \tau_i > 4\xi^2\tau_d \Rightarrow \tau_d < \frac{\tau_i}{4\xi^2} \tag{43}$$

Consequently, we have obtained the same condition for the reset time τ_i as in the previous section (Eqs (18) and (32)-(33)). Assuming that $p = 1$ and that $f > 1$, the derivative time can be obtained from Eqs (33) and (43) as:

$$\tau_d < \frac{\tau_i}{4\xi^2} \Rightarrow \tau_d < \frac{2pf\xi\tau}{4\xi^2} \Rightarrow \tau_d = f_1\frac{pf\tau}{2\xi} \;;\; (f_1 < 1) \tag{44}$$

The self-oscillation frequency can be obtained as function of f and f_1 by substituting Eq (44) into Eq (42), i.e.:

$$\omega_{os} = \frac{1}{\tau}\sqrt{\frac{pf-1}{pf\left(1-pf\cdot f_1\right)}} \Rightarrow \omega_{os\,\min} = \frac{1}{\tau}\sqrt{\frac{pf-1}{pf}} \tag{45}$$

where ω_{osmin} is the minimum value that the self-oscillation frequency can take. It should be noticed that the self-oscillating behavior appears when $f = 1$, and consequently Eq (45) can only be applied when p > 1. Assuming that $p = 1$ -this will be corroborated

ACCEPTED MANUSCRIPT

later- and taking into account that τ is very small, we can choose $f > 1$ very close to unity (for example $f = 1.00001$ to assure acceptable values for the self-oscillation frequency) with $f \cdot f_1 < 1$. Next, we can define the interval of self-oscillation frequencies by $\omega_{os1} > \omega_{osmin}$ and $\omega_{os2} > \omega_{os1}$, so the minimum and maximum allowed values for f_1 will be:

$$f_{1\min} = \frac{1}{f}\left[1 - \frac{f-1}{f\left(\omega_{os1}\tau\right)^2}\right] \;;\; f_{1\max} = \frac{1}{f}\left[1 - \frac{f-1}{f\left(\omega_{os2}\tau\right)^2}\right] \tag{46}$$

With this procedure it is possible to choose an interval for the desired self-oscillation frequencies. Next, the self-oscillation frequency and the parameter τ_d of the PID controller can be obtained by choosing a value for f_1 such that $f_{1min} < f_1 < f_{1max}$. In addition, if one chooses $f >> 1$, the corresponding values for the parameters K_p and τ_i of the PID controller can drive the axis position of the servo to a desired set point, as it will be analyzed in the following section. It is interesting to remark that the describing function is an approximate procedure whose exactitude depends on the F_c filter condition defined by [21]:

$$F_c = \frac{\left|G(3\omega j)G_{PID}(3\omega j)\right|}{\left|G(\omega j)G_{PID}(\omega j)\right|} \tag{47}$$

which can be determined by Eqs (38). The precision of the harmonic balance method is acceptable for $F_c \approx 0.1$.

To validate the relation between $\bar{x}_0$ and U_{1m} given by Eqs (36) and (42) (as well as the numerical simulations of the next section), we are going to deduce how the physical variables defined by Eqs (15-17) and the variables $(\bar{x}, \bar{y})$ in normal form given by Eqs (28) are related. From the Eqs (20) and (21) it is deduced that:

ACCEPTED MANUSCRIPT

For $0<\xi<1$:

$$\begin{bmatrix} x(t) \\ y(t) \\ z(t) \\ w(t) \end{bmatrix} = P_1^{-1} \begin{bmatrix} x_1(t) \\ x_2(t) \\ x_3(t) \\ x_4(t) \end{bmatrix} \Rightarrow \begin{cases} x(t) = p_{112}^{-1} x_2(t) + p_{113}^{-1} x_3(t) + x_4(t) \\ x(t) \equiv \bar{x}(t) \end{cases}$$

For $\xi \geq 1$: (48)

$$\begin{bmatrix} x(t) \\ y(t) \\ z(t) \\ w(t) \end{bmatrix} = P_2^{-1} \begin{bmatrix} x_1(t) \\ x_2(t) \\ x_3(t) \\ x_4(t) \end{bmatrix} \Rightarrow \begin{cases} x(t) = p_{212}^{-1} x_2(t) + p_{213}^{-1} x_3(t) + x_4(t) \\ x(t) \equiv \bar{x}(t) \end{cases}$$

Taking into account the parameter values indicated in table 1, it is obtained that $p_{112}^{-1} \sim 10^{-3}$; $p_{212}^{-1} \sim 10^{-3}$ and $p_{113}^{-1} \sim 10^{-5}$; $p_{213}^{-1} \sim 10^{-5}$, whereas the simulation results indicate~ that $x_2(t) \sim 10^2$ and $x_3(t) \sim 10^3$ (this will be verified next). Therefore, $x(t) \equiv \bar{x}(t) \approx x_4(t)$ and taking into account Eqs (26-28) it is concluded that the output voltage of the PID controller $u_1(t) \equiv x_4(t)$ coincides with the variable associated to the normal form of the BT bifurcation, i.e. $u_1(t) \equiv x_4(t) \approx \bar{x}(t) \equiv x(t)$. Thus for a desired self-oscillation frequency ω_{os}, Eq (36) allows to obtain the period T_{os} from the corresponding initial voltage $\bar{x}_0 \equiv x_0$, which can be compared with the value of U_{1m} deduced from the describing function (Eqs (42)). Consequently, we have an indirect procedure to know the precision of the harmonic balance method for a given value of parameter p.

Assuming that $f = 1 + 10^{-6}$ and $p = 1$ (the time constant is $\tau = 3.7969.10^{-3}$ s), from Eq (45) it is deduced that $\omega_{osmin} = 0.2634$ rad/s, so the arbitrary range $0.3 < \omega_{os} < 3$ rad/s of self-oscillation frequencies can be chosen. If we select $\omega_{os} = 2$ rad/s as the desired self-oscillation frequency, the corresponding value $f_1 = 0.9827$ is deduced from Eq (46) taking $\omega_{os1} = \omega_{os2} = 2$. The parameters of the PID controller can now be obtained as: $K_p = 0.0099$, $\tau_i = 0.0072$ s, $\tau_d = 0.002$ s, $x_0 \equiv \bar{x}_0 = 2.3607$ V and $U_{1m} = 2.3094$ V. In this case, the filter condition given by Eq (47) is $F_c = 0.1111$ and therefore the error of the harmonic balance method can be regarded as acceptable.

ACCEPTED MANUSCRIPT

The previous procedure has been applied to deduce the results shown in Fig 3. Fig 3 a) shows the variation of x_0 and U_{1m} as a function of the self-oscillation frequency for different values of p. The difference between x_0 and U_{1m} is small for large values of p and low values of the self-oscillation frequency. Fig 3 c) shows the filter condition, which is almost independent of the self-oscillation frequency. It should be noted that the harmonic balance method involves an excessive error for $F_c > 0.2$ and for low values of p. In Figs 3 b) and 3 d), the PID parameters are plotted. As expected, the PID parameters are negative without physical meaning for frequencies below ω_{osmin}. On the other hand, since the proportional constant becomes very small for low values of p, the value $p = 1\ V^{-2}s^{-2}$ will be considered in the rest of the paper to avoid this inconvenient.

Figure 3

5. Dynamical analysis of the system by using the Bogdanov-Takens bifurcation

In this section we analyze several dynamical behaviors that can appear as a result of two zero eigenvalues in the matrix associated to the linear part of the servomechanism given by Eqs (15) and (17) [13]. The aim is to corroborate the analytical results and conclusions of the previous section by using numerical simulations. For this purpose, we shall investigate the influence of the parameters K_p, τ_i and τ_d on the self-oscillating regime, the appearance of limit cycles due to the external disturbances and the possibility of chaotic behavior. The simulations are carried by using $0 < \xi < 1$ or $\xi \geq 1$, and in addition, the effect of random noise on the control trajectory (to reach a prescribed set point) will be also analyzed.

5.1 Self-oscillating limit cycles and steady-state regime.

We first analyze the self-oscillation conditions for the servomechanism. Assuming a set point of $\theta_r = 0\ rad$ and $f = 1 + 10^{-6}$, the values $K_p = 0.0099$, $\tau_i = 0.0072\ s$ and $\omega_{osmin} = 0.2634\ rad/s$ are obtained according to the self-oscillation conditions given by Eqs (32) and (33). Next, the frequencies $\omega_{os1} = 0.28\ rad/s$ and $\omega_{os2} = 3\ rad/s$ are chosen with the corresponding values $f_{1min} = 0.1153$ and $f_{1max} = 0.9923$ determined from Eqs (46). By choosing a desired self-oscillation frequency $\omega_{os} = 0.65\ rad/s$, the

ACCEPTED MANUSCRIPT

values $\tau_d = 0.0017$ and $f_1 = 0.8358$ are obtained from Eqs (44) and (46) respectively, and taking $T_{os} = 2\pi/\omega_{os}$ in Eq (36) it follows that $\bar{x}_0 = 0.753\,\mathrm{V}$.

It is important to remark that the self-oscillating behavior depends on the initial condition for the control signal $u_1(0)$. The simulation is carried out equating to zero the initial state variables except for the voltage $x_4(0) \equiv u_1(0) = U_{1m} = 0.7506\ V$, which is calculated taking into account Eq (42) and the self-oscillation condition obtained from the harmonic balance method. It should be noted that this voltage value is very close to the value for $\bar{x}_0$ deduced from Eq (36). The simulation results are shown in Figs 4 a), b) and c), where a limit cycle appears. In Fig 4 d), the power spectral density of the control signal $u_1(t)$ shows that the obtained self-oscillation frequency is 0.6283 rad/s with a relative error of 3.34 %. *At* $t = t_{con} = 50\ s$, a new set point of $\theta_r = 0.8\ rad$ is chosen and the parameter f is changed to $f = 200$ giving rise to new values of K_p ($K_{pc} = 1.9718$) and τ_i ($\tau_{ic} = 1.4428\ s$), whereas τ_d remains unchanged and thus the new set point is reached.

Figure 4

It should be remarked that the possibility of reaching an arbitrary set point only depends on the PID parameter values. However, the values of the PID parameters are independent of the set point, and they only depend on Eqs (33) and (34) deduced from the analysis of the BT bifurcation. This remark is also applicable in the case of the APH bifurcation, which will be analyzed in the next section.

The presence of limit cycles is analyzed assuming that $T_{d2} \neq 0$ and $\theta_{r2} = 0$. In accordance with Eqs (8) and (15), the external disturbance can be written as follows:

$$f_d(t) = \frac{nK_s T_{d2}}{J_{me}} \left[\frac{R_a}{L_a} \sin(\omega_d t) + \omega_d \cos(\omega_d t) \right] \tag{49}$$

Taking into account Eqs (20)-(22) and (49), and neglecting fifth-order terms, Eqs (28) can be written as follows:

ACCEPTED MANUSCRIPT

$$\begin{aligned}\dot{\bar{x}}(t) &= \bar{y}(t) + p_{i13}^{-1} f_p(t) \\ \dot{\bar{y}}(t) &= 3d_1\bar{x}^2(t)\dot{\bar{x}}(t) + d_2\bar{x}^3(t) + p_{i23}^{-1} f_p(t)\end{aligned} \tag{50}$$

where p_{i13}^{-1} and p_{i23}^{-1} are the corresponding elements of the matrices P_1^{-1} and P_2^{-1} defined in Eqs (21), and the indexes i = 1 and i = 2 refer to the cases $0 < \xi < 1$ and $\xi \geq 1$ respectively.

The simulation results are shown in Figs 5 and 6 taking $\xi = 2.5$. Fig 5 a) shows all the state variables $x_i(t)$ *(i = 1, 2, 3, 4)*, in which it can be observed that $x_2(t)$ and $x_3(t)$ are lower than 40 (the maximum values of $x_2(t)$ and $x_3(t)$ are *8.4004* and *38.4869* respectively) whereas $p_{212}^{-1} = 4.7594 \cdot 10^{-3}$ and $p_{213}^{-1} = 1.0452 \cdot 10^{-5}$. Consequently, Eq (48) allows to deduce that $x(t) \approx x_4(t)$. As shown in Fig 5 b), we first choose θ_r *= 1 rad, f = 5 (f > 1)* to obtain asymptotic stability for the values of K_p and τ_i deduced from Eqs (33). The value of τ_d has been chosen in accordance with Eq (44) taking f_1 *= 0.4* so that $\tau_d = \tau/\xi$.

At t_p *= 10 s*, an external disturbance torque of $T_d(t) = 4.567\sin(1.234t)$ N is applied and the system jumps to a limit cycle (both t_p and $T_d(t) = 4.567\sin(1.234t)$ have been chosen arbitrarily). At $t = t_{con}$ *= 60 s*, we select a new set point of θ_r *= 0.5 rad,* the value of *f* is increased to *f = 10* with the corresponding updated values of K_p and τ_i. To check the robustness of the PID controller, it is assumed that the system can exhibit random noise, i.e. the state variables are corrupted with a noise signal *n(t)* defined by (see Fig 1):

$$\begin{aligned} x_1(t) &= x_1(t) + f_{na}[X - 0.5] \;\; ; \;\; x_2(t) = x_2(t) + f_{na}[X - 0.5] \\ x_3(t) &= x_3(t) + f_{na}[X - 0.5] \;\; ; \;\; x_4(t) = x_4(t) + f_{na}[X - 0.5] \end{aligned} \tag{51}$$

where *X* is a random variable that is uniformly distributed between 0 and 1, and $f_{na} > 0$ is an amplification factor to obtain a uniformly distributed noise amplitude between $-f_{na}/2$ and $f_{na}/2$. It is assumed that random noise with f_{na} *= 0.2* is present for $t \geq t_{con} = 60$. As shown in Fig 5 b), it is clear that the set point is reached even with a disturbance torque and random noise. In Fig 5 c), the variables $u_1(t)$ and x(t) are plotted, and it can

ACCEPTED MANUSCRIPT

be observed that $u_1(t) \approx x(t)$ in accordance with the previous reasoning. On the other hand, Fig 5 d) allows to verify that the outlined procedure provides a physically feasible armature current $i_a(t)$ in the context of the considered system.

Fig 6 a) shows two limit cycles. One of them is obtained from Eqs (15) and it is plotted with $u_1(t) = x_4(t)$, whereas its derivative $du_1(t)/dt$ is numerically obtained from $\dot{x}_4(t)$ within the integration scheme. The other limit cycle is plotted with the variables $\left[\bar{x}(t), \bar{y}(t) \equiv \dot{\bar{x}}(t)\right]$ deduced from Eqs (50). A high degree of concordance between both cycles can be observed. In addition, Fig 6 b) shows the plots of du_1/dt and $d\bar{x}(t)/dt$ as a function of the time, where the noise signal has been added after the control has been applied. As it can be observed, the analytical deductions are reasonably in accordance with the numerical results.

Figure 5

Figure 6

5.2 Analysis of the chaotic behavior

It is well known that a nonlinear system in self-oscillating regime can reach chaotic behavior when an external harmonic disturbance is applied [17-19]. To investigate this issue we apply the general Eqs (15), which account for a possible external disturbance $T_d(t)$ and an harmonic input $\theta_r(t)$ defined by Eqs (8). In particular, taking into account the state variables defined in Eqs (16) and assuming that $T_d(t) = 0$, the simulation results obtained from Eqs (15) are shown in Fig 7. It is interesting to remark that the values of the PID parameters for t < 50 s have been chosen in accordance with Eqs (33), and (44) taking $p = 1$, $f = 1 + 10^{-6}$ and $f_1 = 0.9827$, so the system has self-oscillating behavior. At $t = t_r \geq 50\ s$ the input is changed to $\theta_r(t) = 1 + 0.987 \sin 0.789t$, which leads to the appearance of chaotic behavior. In this case, the system is not autonomous and thus it is transformed into an autonomous one by introducing an auxiliary variable $x_5(t)$ defined as:

$$\frac{dx_5(t)}{dt} = \omega_r \ \ ; \ \ x_5(t) \mod 2\pi \tag{52}$$

ACCEPTED MANUSCRIPT

Figs 7 a) and 7 b) show strange attractors both in the phase plane *u(t)-du(t)/dt* and *θ(t)-dθ(t)/dt* respectively.

Figure 7

To corroborate that the strange attractors of Fig 7 are chaotic, the simulation results of two simulations of the same state variable with very close initial conditions (denoted by $x_1(t)$ and $x_{11}(t)$) are plotted in Fig 8 a). It should be noted that the simulation results are completely different at *t = 190 s* approximately, and therefore the system shows a strong sensitive dependence. Fig 8 b) shows the error evolution as function of the time, which corroborates the results of Fig 8 a). In Fig 8 c) all Lyapunov exponents have been calculated [35-36] showing that one of them is positive, which provides another indicator of chaotic behavior. Since the numerical procedure may be unstable, the Runge-Kutta-Fehlberg integration method has been used with a simulation step of 0.002 s. The divergence of the vector field is obtained from Eqs (15), (17) and (52) as:

$$div\vec{f} = -\frac{2\xi}{\tau} = -500.4044 \tag{53}$$

whereas the sum of Lyapunov exponents in steady state is given by:

$$LY_e = \begin{bmatrix} 0.0783 & -0.1085 & -250.1975 & -250.1639 & 0 \end{bmatrix}$$
$$\sum LY_e = -500.3916 \tag{54}$$

The divergence value of Eq (53) is approximately equal to the sum of the steady-state Lyapunov exponents given in Eq (54), which also corroborates the accurateness of the numerical computations. On the other hand, Fig 8 d) shows that the power spectral density exhibits a broad spectrum with decaying energy, which is a typical feature of chaotic systems [34].

Figure 8

ACCEPTED MANUSCRIPT

Figs 9 a) and b) show the auxiliary variable defined in Eq (52) as a function of the state variables $x_1(t)$ and $x_2(t)$, for which the corresponding Poincaré sections in Figs 9 c) and 9 d) with $f_{\omega 1} = 3$ and $f_{\omega 2} = 1$ show a clear chaotic behavior. Additionally, two bifurcation diagrams have been calculated in Fig 10 by using the numerical algorithm of Ref [37]. In Fig 10 a) it is assumed that $\theta_{r1} = 0$ and $T_d(t) \equiv 0$, whereas in Fig 10 b) we have that $\theta(t) \equiv 0$, $T_{d1} = 0$ and $T_{d2} = 2.55$ N.m. The presence of a sequence of windows with chaotic and multi-periodic behaviors can be clearly appreciated in both cases.

Figure 9

Figure 10

To illustrate how the chaotic behavior can be used, we consider the data shown in legend of Fig 10 a), in which a chaotic window appears for $\theta_{r1} = 0$, $\theta_{r2} = 1.234$, $\omega_r = 1.125$ rad/s and $T_d(t) \equiv 0$. If we assume a desired set point inside a zone of the strange attractor, as a result of its characteristic tangle (see Fig 7) we can affirm that a chaotic trajectory will pass very near this point after a certain simulation time. When this occurs, the parameters of the PID controller can be changed to reach the set point with a very small control effort.

In Fig 11 a) the phase plane $\theta(t)$-$d\theta(t)/dt$ is plotted, in which we define the capture region $\Omega \equiv (r_{ax} = 0.5, r_{ay} = 0.4)$ around the set point $\theta_r = 0.45$ rad containing the points A and B. When a chaotic trajectory enters the capture region Ω after the arbitrary time $t_{con} = 250$ s, the control law is changed taking f = 150 and the new PID controller parameters are determined in accordance with Eqs (33) and (44). As shown in Fig 11 b), it is clear that the capture zone is reached at $t_{con1} = 255.455$ s, i.e. 5.455 s after the control law has been changed at $t_{con} = 250$ s. Fig 11 c) shows the control effort, which is clearly smaller than when the control law is changed at exactly $t_{con} = 250$ s.

Figure 11

6. Analysis of the Andronov-Poincaré-Hopf bifurcation

As we saw in section 2, the constant term T_{d1} of the disturbance torque (Eqs (8)) was assumed to be zero and consequently Eqs (17) allowed to deduce that a BT

ACCEPTED MANUSCRIPT

bifurcation appeared. In this section we shall investigate the possibility of the appearance of an APH bifurcation when $T_{d1} \neq 0$, for which Eqs (14) will be taken into account. For this purpose, we assume that $\theta_{r2} = 0$ and we introduce the state variables defined as:

$$y_1(t)=\theta(t)\ ;\ y_2(t)=\frac{d\theta(t)}{dt}\ ;\ y_3(t)=\frac{d^2\theta(t)}{dt^2}\ ;\ y_4(t)=u_1(t) \tag{55}$$

According to Eq (55), Eqs (14) can be rewritten as follows:

$$\begin{bmatrix}\dot{y}_1(t)\\ \dot{y}_2(t)\\ \dot{y}_3(t)\\ \dot{y}_4(t)\end{bmatrix}=\begin{bmatrix}0 & 1 & 0 & 0\\ 0 & 0 & 1 & 0\\ 0 & -1/\tau^2 & -2\xi/\tau & 0\\ -K_pK_s/\tau_i & -K_pK_s & -K_pK_s\tau_d & 0\end{bmatrix}\begin{bmatrix}y_1(t)\\ y_2(t)\\ y_3(t)\\ y_4(t)\end{bmatrix}+\begin{bmatrix}0\\ 0\\ K'K_{ne}x_4^3(t)/\tau^2-nR_aT_{d1}/J_{me}L_a\\ K_pK_s\theta_{r1}/\tau_i\end{bmatrix} \tag{56}$$

Taking into account Eqs (13), the equilibrium points of the system are given by:

$$y_{1e}=\theta_{r1}\ ;\ y_{2e}=0\ ;\ y_{3e}=0\ ;\ y_{4e}=\begin{cases}\left(\dfrac{R_aT_{d1}}{K_mK_aK_{ne}}\right)^{1/3} & \text{for } T_{d1}>0\\ -\left(\dfrac{R_aT_{d1}}{K_mK_aK_{ne}}\right)^{1/3} & \text{for } T_{d1}<0\end{cases} \tag{57}$$

Introducing the deviation variables:

$$y_1'(t)=y_1(t)-\theta_{r1}\ ;\ y_2'(t)=y_2(t)\ ;\ y_3'(t)=y_3(t)\ ;\ y_4'(t)=y_4(t)-y_{4e} \tag{58}$$

into Eqs (56) and taking into account Eqs (57), the following equations are deduced:

$$\begin{bmatrix}\dot{y}_1'(t)\\ \dot{y}_2'(t)\\ \dot{y}_3'(t)\\ \dot{y}_4'(t)\end{bmatrix}=\begin{bmatrix}0 & 1 & 0 & 0\\ 0 & 0 & 1 & 0\\ 0 & -1/\tau^2 & -2\xi/\tau & 3K_\theta y_{4e}^2\\ -K_{ps}/\tau_i & -K_{ps} & -K_{ps}\tau_d & 0\end{bmatrix}\begin{bmatrix}y_1'(t)\\ y_2'(t)\\ y_3'(t)\\ y_4'(t)\end{bmatrix}+\begin{bmatrix}0\\ 0\\ 3K_\theta y_{4e}y_4'^2+K_\theta y_4'^3\\ 0\end{bmatrix} \tag{59}$$

being $K_{ps}=K_pK_s\ ;\ K_\theta=K'K_{ne}/\tau^2$. The eigenvalues of the linear part of Eq (59) are the roots of the characteristic equation defined as:

ACCEPTED MANUSCRIPT

$$\lambda^4 + a_3\lambda^3 + a_2\lambda^2 + a_1\lambda + a_0 = 0$$
$$a_3 = \frac{2\xi}{\tau}\ ;\ a_2 = \frac{1}{\tau^2} + 3K_\theta y_{4e}^2 \tau_d K_{ps}\ ;\ a_1 = 3K_\theta y_{4e}^2 K_{ps}\ ;\ a_0 = 3K_\theta y_{4e}^2 \frac{K_{ps}}{\tau_i} \tag{60}$$

where $K_{ps} = K_p K_s$. Since $a_i > 0$ *(i = 1,2,3,4)*, from the Routh criterion of stability [24] it is deduced that an APH bifurcation appears if the following self-oscillation conditions are fulfilled:

$$a_2 a_3 - a_1 > 0\ \ ;\ \ a_1 a_2 a_3 - a_1^2 - a_0 a_3^2 = 0 \tag{61}$$

From Eqs (60) and (61) it is deduced that:

$$a_2 a_3 - a_1 > 0 \Rightarrow \frac{2\xi}{\tau^3} > 3K_\theta y_{4e}^2 K_{ps}\left(1 - \tau_d \frac{2\xi}{\tau}\right) \Rightarrow \begin{cases} \tau_d = f_d \dfrac{\tau}{2\xi}\ ;\ f_d < 1 \\ K_{ps} < \dfrac{2\xi}{3K_\theta y_{4e}^2 \tau^3 (1 - f_d)} \end{cases} \tag{62}$$

where the parameter f_d is introduced to rewrite the inequalities of Eq (62) in term of equalities, i.e.:

$$a_1 a_2 a_3 = a_1^2 + a_0 a_3^2 \Rightarrow \frac{2\xi}{\tau^2}\left(\frac{1}{\tau} - \frac{2\xi}{\tau_i}\right) = 3K_\theta y_{4e}^2 K_{ps}(1 - f_d) \tag{63}$$

From Eqs (62) and (63) it is possible to deduce the parameter values of the PID controller to obtain a self-oscillating behavior associated to an APH bifurcation, i.e.:

$$\tau_d = f_d \frac{\tau}{2\xi}\ \ ;\ \ K_{ps} = f_k \frac{2\xi}{3K_\theta y_{4e}^2 \tau^3 (1 - f_d)}\ \ ;\ \ \tau_i = \frac{2\xi\tau}{1 - f_k} \tag{64}$$

where $f_k < 1$ is another (positive) parameter that has been introduced to transform the last inequality of Eqs (62) into the second equality of Eq (64). In addition, the self-oscillation frequency is given by:

$$\omega_{aph}^2 = \frac{a_0 a_3}{a_2 a_3 - a_1} \Rightarrow \omega_{aph}^2 = \frac{3K_\theta y_{4e}^2 \tau K_{ps}}{2\xi} \Rightarrow \omega_{aph} = \frac{1}{\tau}\sqrt{\frac{f_k}{1 - f_d}} \tag{65}$$

ACCEPTED MANUSCRIPT

Once the pair of pure imaginary roots of Eqs (60) given by $\lambda_{1,2} = \pm j\omega_{aph}$ are known, the other roots can be determined by inspection of the polynomial given by Eq (60), i.e.:

$$\lambda_{3,4} = -\frac{\xi}{\tau} \pm \sqrt{\frac{\xi^2}{\tau^2} - \left(\frac{1-f_k}{\tau^2}\right)} \Rightarrow \begin{cases} \text{Two complex conjugate roots if } \xi^2 < 1-f_k \\ \text{Two real roots if } \xi^2 > 1-f_k \end{cases} \quad (66)$$

It should be remarked that the difference between the BT and APH bifurcations relies on the fact that the BT bifurcation appears when the disturbance torque is zero ($T_d(t) \equiv 0$), whereas a nonzero constant torque $T_d(t) = T_{d1} \neq 0$ is a necessary but not sufficient condition for the appearance of the APH bifurcation. In this case, the sufficient conditions to obtain an APH bifurcation are given by Eqs (61)-(63).

The following step of our analysis consists of investigating the stability conditions for the APH bifurcation. For this purpose, it is necessary to determine the first Lyapunov value for the weak focus associated to $\lambda_{1,2} = \pm j\omega_{aph}$ [14-16], [24]. Since the analytical calculations lead to voluminous formulae, it is preferable to use the computational procedure shown in Appendix. Whereas a first Lyapunov value $L_1>0$ leads to an unstable weak focus, a negative value $L_1<0$ leads to a stable weak focus whose trajectory length in the phase plane tends to infinite while turning around the weak focus [24].

In accordance with the computational procedure shown in the Appendix, the first Lyapunov value in Fig 12 has been calculated as a function of f_k taking T_{d1} as a parameter. Since the value of τ is small (see Table 1), the value of f_k must also be small to obtain admissible values for the self-oscillation frequency (Eq (65)). The first Lyapunov values shown in Figs 12 a) and b) have been obtained for $\xi = 0.95$ and $\xi = 5$ respectively, which according to Eq 66 imply complex conjugate roots for $\xi = 0.95$ and real negative roots for $\xi = 5$.

Figure 12

ACCEPTED MANUSCRIPT

To corroborate the previous results, the system has been simulated with PID parameter values so that the self-oscillation conditions are fulfilled according to Eqs (64). For $\xi = 0.95$, $T_{d1} = 9$ N.m and $f_k = 1.2.10^{-4}$, the first Lyapunov value depicted in Fig 12 a) is $L_1 = 1.0881.10^{-4}$, which is positive although very small. Since the value $L_1 > 0$ can be considered as a measure of the divergence speed of trajectories spiraling away the weak focus, a long simulation time (higher than 10^4 s) will be necessary to appreciate the divergence effect. In accordance with Eq (65), the self-oscillation frequency is $\omega_{aph} = 6.4512$ rad/s for $f_k = 1.2.10^{-4}$ and $f_d = 0.8$.

The simulation results are plotted in Fig 13. Figs 13 a) and b) show the limit cycles while Figs 13 c) and d) show the control signal and the armature current in the DC motor respectively. To corroborate the calculations shown in the appendix in accordance with the results shown in Fig 12 b), Fig 14 shows unstable and stable weak focus that appear as a result of the APH bifurcation for $\xi = 5 > 1$. As shown in Figs 14 a) and b), a positive Lyapunov value ($L_1 = 12.6337$) is obtained for $T_{d1} = 0.03$ N and $f_k = 1.2.10^{-3}$, so an unstable weak focus appears. Fig 14 c) shows a stable weak focus ($L_1 <0$) that has been obtained by using Fig 12 b) with $T_{d1} = 0.51$ N and $f_k = 6.10^{-3}$, and its corresponding armature current is depicted in Fig 14 d). It should be remarked that the effects of instability or stability are clearly visible even for small (positive or negative) values of the first Lyapunov value.

Figure 13

Figure 14

Once the self-oscillating behavior has been corroborated, the appearance of chaotic behavior is investigated by assuming a harmonic disturbance torque with $T_{d2} = 10$ N.m and $\omega_p = \omega_{aph}/2 = 3.2256$ rad/s at an arbitrary time t = 10 s, as well as a constant reference angle $\theta_{r1} = 1$ rad with $\theta_{r2} =0$. As in the case of the BT bifurcation, the presence of a positive Lyapunov exponent together with the Poincaré section and the power spectral density allow to assure the appearance of a new family of strange attractors, which has been used to investigate how an arbitrary set point can be reached. For this purpose, a capture region Ω ($r_{ax} = 0.3$, $r_{ay} = 0.2$) is defined around the set point $\theta_r = 0.45$ rad. Consequently, when a chaotic trajectory enters the region Ω after $t_{con} = 250$ s, the

ACCEPTED MANUSCRIPT

PID controller parameters will be changed to destroy the chaotic dynamics and reach the set point even in presence of noise (see Eqs (51)).

The simulation results together with the corresponding parameter values are indicated in Fig 15. Fig 15 a) shows the sensitive dependence of the variable $u(t) \equiv u_{11}(t)$ when the initial error in the initial conditions of system is 10^{-8} (Eqs (16)). It should be noted that, when the parameters of the PID controller are changed (the control action begins at t = 250.98), the values of both variables are almost coincident after a transitory. Fig 15 b shows the position of motor shaft, which allows to appreciate that the system is almost self-oscillating for t < 10 s -i.e. before the disturbance is applied-. Fig 15 c) shows the control trajectory plus noise (with $f_{na} = 0.1$) embedded in a sea of chaotic trajectories. It should be noted that the PID controller drives the motor shaft to the set point $\theta_r = 0.45\ rad$ following the control trajectory in presence of noise.

Figure 15

The APH bifurcation is investigated in Figs 16 and 17 taking $\xi = 5$. In this case, we assume that $T_{d1} = 0.52\ N$, $f_d = 0.8$ and $f_k = 2.5.10^{-3}$ to obtain a stable weak focus in accordance with Figs 12 b) ($L_1 = -0.049$) and Figs 14 c) and d). The PID parameter values and the self-oscillation frequency are deduced from Eqs (64) and (65). From Eq (66) it follows that the eigenvalues $\lambda_{3,4}$ are real. The external disturbance is applied at t = 10 s assuming that $T_{d2} = 0.45$ N and $\omega_p = \omega_{aph}/2 = 2.7973$ rad/s, for which another family of strange attractors appears. At t = 250 s, the PID parameters are changed and a chaotic orbit intersect the capture zone Ω 1.81 s later. Fig 16 a) shows a strange attractor in the u(t)-du(t)/dt phase plane. Figs 16 b) and c) show the control signal generated by the PID controller and the position of the motor shaft respectively. The armature current is shown in Fig 16 d), whereas the strange attractor in the phase plane $\theta(t)$-$d\theta(t)/dt$ as well as the control trajectory plus noise are plotted in Fig 17.

Figure 16

Figure 17

The same remark regarding the BT bifurcation can be made in case of the APH bifurcation, i.e.: the values of the PID parameters are independent of the set point;

ACCEPTED MANUSCRIPT

however, a set point may only be reached if the parameters values of the PID controller are suitably chosen.

Finally, it is interesting to remark that the control technique used in the work of Ott, Gregobi and Yorke [38] is applied to a bidimensional map whose chaotic trajectory is linearized around the set point to apply the control effort when the chaotic trajectory is close to the set point. However the goal of this paper is different, since we pretend to use a PID controller to drive the motor shaft to a predetermined set point. For this reason, the previous control technique has not been used in this paper.

7 Conclusions

The nonlinear dynamics of a PID controlled servomechanism aimed to stabilize an external body subjected to a constant disturbance torque has been investigated in this paper. By using a cubic nonlinearity and a PID feedback control system, it has been shown that the matrix of the linear part of the system can have two zero eigenvalues or two pure complex eigenvalues which are responsible for BT and APH bifurcations respectively. It has been verified that the BT bifurcation is more robust than the APH one against harmonic external disturbances applied to the load.

The analysis of the BT bifurcation together with the center manifold theorem has allowed us to obtain a simplified system which can be used to choose appropriate values for the proportional constant K_p and the reset time τ_i of the PID controller. On the other hand, the derivative time τ_d and a predefined interval of self-oscillation frequencies have been obtained through the describing function of the cubic nonlinearity. In addition, it has been corroborated that harmonic variations in the reference input can produce chaotic oscillations, which have been studied through the analysis of the sensitive dependence, Lyapunov exponents, Poincare sections and bifurcation diagrams.

We have demonstrated that the chaotic behavior can be used jointly with the PID controller in an advantageous manner. For this purpose, we define a small capture zone around the desired set point and the so called control action is applied when a chaotic trajectory intersects such capture zone. The control action consists of a change in the

ACCEPTED MANUSCRIPT

PID parameters K_p, τ_i and τ_d which allows to reach the set point by using very small control signals. The correct performance of the PID controller has been corroborated even in the presence of random noise.

The analysis of the APH bifurcation has been carried out assuming that a constant external disturbance is applied to the load. The Routh stability criterion has allowed to deduce the conditions which give two pure imaginary eigenvalues, the self-oscillation frequency and the PID controller parameters. The stability of the weak focus associated to the self-oscillating behavior has been investigated through the calculation of the first Lyapunov value L_1. It has been verified that the simulation results are in accordance with the sign (positive or negative) obtained for L_1. For positive values of L_1, the chaotic behavior has also been found and used as in the case of the BT bifurcation. It should however be noted that the families of strange attractors for the BT and APH bifurcations are different.

Our analysis has provided a unified framework in which PID control, BT and APH bifurcations, describing function, Lyapunov stability theory, chaotic behavior, random noise and calculation of the first Lyapunov value have allowed to tune the PID parameters with a better understanding of the underlying dynamical behaviors. The methodology presented in this paper can be extended to more sophisticated systems with more complicated control laws, which in turn can result in new interesting dynamical behaviors.

Appendix

In this Appendix, a computational procedure to obtain the first Lyapunov value is developed. For this purpose we will distinguish the cases in which the eigenvalues $\lambda_{3,4}$ are complex (case (a)) or real and negative (case (b)).

a) A pair of complex conjugate eigenvalues:

$$\lambda_{1,2} = \pm j\omega_{aph} \;\; ; \;\; \lambda_{3,4} = \alpha \pm j\omega_h \;\; ; \;\; \alpha = -\xi/\tau \;\; ; \;\; \omega_h = \sqrt{(1-f_k)-\xi^2}\,\Big/\tau \qquad \text{(A1)}$$

- Step1

ACCEPTED MANUSCRIPT

Let P_a be the matrix that transforms the linear part of Eqs (59) into its Jordan canonical form. The columns of P_a are then the eigenvectors associated to the eigenvalues of linear part of Eqs (59), so it follows that:

$$y' = P_a \bar{y} \Rightarrow \begin{bmatrix} y_1' \\ y_2' \\ y_3' \\ y_4' \end{bmatrix} = \begin{bmatrix} 0 & 1 & 0 & 1 \\ \omega_{aph} & 0 & \omega_h & \alpha \\ 0 & -\omega_{aph}^2 & n_2 & m_2 \\ n_1 & -K_{ps} & n_3 & m_3 \end{bmatrix} \begin{bmatrix} \bar{y}_1 \\ \bar{y}_2 \\ \bar{y}_3 \\ \bar{y}_4 \end{bmatrix} \begin{cases} m_2 = \alpha^2 - \omega_h^2 \\ n_2 = 2\alpha\omega_h \\ m_3 = \dfrac{-\left(K_{ps}/\tau_i\right)\alpha}{\alpha^2 + \omega_h^2} - K_{ps} - \alpha\tau_d K_{ps} \\ n_3 = \dfrac{\left(K_{ps}/\tau_i\right)\omega_h}{\alpha^2 + \omega_h^2} - \omega_h\tau_d K_{ps} \end{cases} \tag{A2}$$

- Step2

From the new coordinates given by Eqs (A2), the equations of the system (59) can be written in its Jordan canonical form as follows:

$$\begin{bmatrix} \dot{\bar{y}}_1 \\ \dot{\bar{y}}_2 \\ \dot{\bar{y}}_3 \\ \dot{\bar{y}}_4 \end{bmatrix} = \begin{bmatrix} 0 & -\omega_{aph} & 0 & 0 \\ \omega_{aph} & 0 & 0 & 0 \\ 0 & 0 & \alpha & -\omega_h \\ 0 & 0 & \omega_h & \alpha \end{bmatrix} \begin{bmatrix} \bar{y}_1 \\ \bar{y}_2 \\ \bar{y}_3 \\ \bar{y}_4 \end{bmatrix} + P_a^{-1} \begin{bmatrix} 0 \\ 0 \\ f_3' \\ 0 \end{bmatrix} \tag{A3}$$

$$f_3' = \gamma\left(n_1\bar{y}_1 - K_{ps}\bar{y}_2 + n_3\bar{y}_3 + m_3\bar{y}_4\right)^2 + K_\theta\left(n_1\bar{y}_1 - K_{ps}\bar{y}_2 + n_3\bar{y}_3 + m_3\bar{y}_4\right)^3$$

where from Eqs (59) it follows that $\gamma = 3K_\theta y_{4e}$. Taking into account the center manifold theorem, the variables $\left(\bar{y}_3, \bar{y}_4\right)$ can be approximated by:

$$h\left(\bar{y}_1, \bar{y}_2\right) = \begin{bmatrix} h_1\left(\bar{y}_1, \bar{y}_2\right) \\ h_2\left(\bar{y}_1, \bar{y}_2\right) \end{bmatrix} \Rightarrow \begin{cases} \bar{y}_3 = a_1\bar{y}_1^2 + a_2\bar{y}_2^2 + a_3\bar{y}_1\bar{y}_2 \\ \bar{y}_4 = b_1\bar{y}_1^2 + b_2\bar{y}_2^2 + b_3\bar{y}_1\bar{y}_2 \end{cases} \tag{A4}$$

The function f'_3 in Eqs (A3) can be expressed by using only terms up to third order, so it follows that:

ACCEPTED MANUSCRIPT

$$
\begin{aligned}
&f_3' = t_{20}\bar{y}_1^2 + t_{02}\bar{y}_2^2 + t_{11}\bar{y}_1\bar{y}_2 + t_{30}\bar{y}_1^3 + t_{21}\bar{y}_1^2\bar{y}_2 + t_{12}\bar{y}_1\bar{y}_2^2 + t_{03}\bar{y}_2^3 \\
&t_{20} = \gamma n_1^2 \;\; ; \;\; t_{02} = \gamma K_{ps}^2 \;\; ; \;\; t_{11} = -2\gamma n_1 K_{ps} \\
&t_{30} = \gamma\left(2n_1 n_3 a_1 + 2n_1 m_3 b_1\right) + K_\theta n_1^3 \;\; ; \;\; t_{03} = \gamma\left(-2K_{ps} n_3 a_2 - 2K_{ps} m_3 b_2\right) - K_\theta K_{ps}^3 \\
&t_{12} = \gamma\left(2n_1 n_3 a_3 + 2n_1 m_3 b_3 - 2K_{ps} n_3 a_1 - 2K_{ps} m_3 b_1\right) - 3K_\theta n_1^2 K_{ps} \\
&t_{21} = \gamma\left(2n_1 n_3 a_2 + 2n_1 m_3 b_2 - 2K_{ps} n_3 a_3 - 2K_{ps} m_3 b_3\right) + 3K_\theta n_1 K_{ps}^2
\end{aligned}
\tag{A5}
$$

On the other hand, from Eqs (A3) it is obtained that:

$$
P_a^{-1}\begin{bmatrix} 0 \\ 0 \\ f_3' \\ 0 \end{bmatrix} = \begin{bmatrix} \bar{f}_1 \\ \bar{f}_2 \\ \bar{f}_3 \\ \bar{f}_4 \end{bmatrix} = \begin{bmatrix} P_{a13}^{-1} f_3' \\ P_{a23}^{-1} f_3' \\ P_{a33}^{-1} f_3' \\ P_{a34}^{-1} f_3' \end{bmatrix} \tag{A6}
$$

where:

$$
\begin{aligned}
\bar{f}_1 &= a_{20}^1\bar{y}_1^2 + a_{02}^1\bar{y}_2^2 + a_{11}^1\bar{y}_1\bar{y}_2 + a_{30}^1\bar{y}_1^3 + a_{21}^1\bar{y}_1^2\bar{y}_2 + a_{12}^1\bar{y}_1\bar{y}_2^2 + a_{03}^1\bar{y}_2^3 \\
\bar{f}_2 &= a_{20}^2\bar{y}_1^2 + a_{02}^2\bar{y}_2^2 + a_{11}^2\bar{y}_1\bar{y}_2 + a_{30}^2\bar{y}_1^3 + a_{21}^2\bar{y}_1^2\bar{y}_2 + a_{12}^2\bar{y}_1\bar{y}_2^2 + a_{03}^2\bar{y}_2^3 \\
\bar{f}_3 &= a_{20}^3\bar{y}_1^2 + a_{02}^3\bar{y}_2^2 + a_{11}^3\bar{y}_1\bar{y}_2 + a_{30}^3\bar{y}_1^3 + a_{21}^3\bar{y}_1^2\bar{y}_2 + a_{12}^3\bar{y}_1\bar{y}_2^2 + a_{03}^3\bar{y}_2^3 \\
\bar{f}_4 &= a_{20}^4\bar{y}_1^2 + a_{02}^4\bar{y}_2^2 + a_{11}^4\bar{y}_1\bar{y}_2 + a_{30}^4\bar{y}_1^3 + a_{21}^4\bar{y}_1^2\bar{y}_2 + a_{12}^4\bar{y}_1\bar{y}_2^2 + a_{03}^4\bar{y}_2^3
\end{aligned}
\tag{A7}
$$

and:

$$
a_{ij}^1 = P_{a13}^{-1} t_{ij} \;\; ; \;\; a_{ij}^2 = P_{a23}^{-1} t_{ij} \;\; ; \;\; a_{ij}^3 = P_{a33}^{-1} t_{ij} \;\; ; \;\; a_{ij}^4 = P_{a43}^{-1} t_{ij} \tag{A8}
$$

whereas the terms P_{a13}^{-1} , P_{a23}^{-1} , P_{a33}^{-1} and P_{a43}^{-1} are determined from the inverse matrix of P_a.

- Step 3

The calculation of the coefficients a_i and b_i (i = *1,2,3*) given in Eqs (A4) is carried out by applying the center manifold theorem as follows:

$$
\begin{aligned}
&D_{\bar{y}} h\left(\bar{y}_1, \bar{y}_2\right)\left\{A\bar{y} + f\left[\bar{y}_1, \bar{y}_2, h\left(\bar{y}_1, \bar{y}_2\right)\right]\right\} = Bh\left(\bar{y}_1, \bar{y}_2\right) + g\left[\bar{y}_1, \bar{y}_2, h\left(\bar{y}_1, \bar{y}_2\right)\right] \\
&\bar{y} = \begin{bmatrix} \bar{y}_1 \\ \bar{y}_2 \end{bmatrix} \;\; ; \;\; A = \begin{bmatrix} 0 & -\omega_{aph} \\ \omega_{aph} & 0 \end{bmatrix} \;\; ; \;\; f\left[\bar{y}_1, \bar{y}_2, h\left(\bar{y}_1, \bar{y}_2\right)\right] = \begin{bmatrix} \bar{f}_1 \\ \bar{f}_2 \end{bmatrix} \;\; ; \;\; B = \begin{bmatrix} \alpha & -\omega_h \\ \omega_h & \alpha \end{bmatrix} \\
&g\left[\bar{y}_1, \bar{y}_2, h\left(\bar{y}_1, \bar{y}_2\right)\right] = \begin{bmatrix} \bar{f}_3 \\ \bar{f}_4 \end{bmatrix} \;\; ; \;\; D_{\bar{y}} h\left(\bar{y}_1, \bar{y}_2\right) = \begin{bmatrix} 2a_1\bar{y}_1 + a_3\bar{y}_2 & 2a_2\bar{y}_2 + a_3\bar{y}_1 \\ 2b_1\bar{y}_1 + b_3\bar{y}_2 & 2b_2\bar{y}_2 + b_3\bar{y}_1 \end{bmatrix}
\end{aligned}
\tag{A9}
$$

ACCEPTED MANUSCRIPT

It should be noted that the product: $D_{\bar{y}}h(\bar{y}_1,\bar{y}_2)\,f\left[\bar{y}_1,\bar{y}_2,h(\bar{y}_1,\bar{y}_2)\right]$ gives terms of third and fourth order in the variables $(\bar{y}_1,\bar{y}_2)$, which are not necessary in the calculation of the coefficients a_i and b_i. By identifying terms coefficients of $\bar{y}_1^2,\bar{y}_2^2$ and $\bar{y}_1\bar{y}_2$ in both members of Eq (A9), the following system of equations can be written in matrix form:

$$\begin{bmatrix} \alpha & 0 & \omega_{aph} & \omega_h & 0 & 0 \\ -\omega_h & 0 & 0 & \alpha & 0 & \omega_{aph} \\ 0 & \alpha & -\omega_{aph} & 0 & \omega_h & 0 \\ 0 & -\omega_h & 0 & 0 & \alpha & -\omega_{aph} \\ -2\omega_{aph} & 2\omega_{aph} & \alpha & 0 & 0 & \omega_h \\ 0 & 0 & -\omega_h & -2\omega_{aph} & 2\omega_{aph} & \alpha \end{bmatrix} \begin{bmatrix} a_1 \\ a_2 \\ a_3 \\ b_1 \\ b_2 \\ b_3 \end{bmatrix} = \begin{bmatrix} a_{20}^3 \\ a_{20}^4 \\ a_{02}^3 \\ a_{02}^4 \\ a_{11}^3 \\ a_{11}^4 \end{bmatrix} \tag{A10}$$

Consequently, the coefficients a_i and b_i can be calculated by resolving the matrix equation (A10).

- Step 4

From Eqs (A3) and (A6), the approximate system reduced to the center manifold can be written as follows:

$$\begin{bmatrix} \dot{\bar{y}}_1 \\ \dot{\bar{y}}_2 \end{bmatrix} = \begin{bmatrix} 0 & -\omega_{aph} \\ \omega_{aph} & 0 \end{bmatrix} \begin{bmatrix} \bar{y}_1 \\ \bar{y}_2 \end{bmatrix} + \begin{bmatrix} \bar{f}^1 \\ \bar{f}^2 \end{bmatrix} + \mathrm{O}\left\|(\bar{y}_1,\bar{y}_2)^4\right\| \;;\; \begin{bmatrix} \bar{f}^1 \\ \bar{f}^2 \end{bmatrix} \equiv \begin{bmatrix} \bar{f}_1 \\ \bar{f}_2 \end{bmatrix} \tag{A11}$$

The first Lyapunov value is calculated as [43-44]:

$$L_1 = \frac{1}{16}\left[\bar{f}^1_{y_1y_1y_1} + \bar{f}^1_{y_1y_2y_2} + \bar{f}^2_{y_1y_1y_2} + \bar{f}^2_{y_2y_2y_2}\right] + \frac{1}{16\omega_{aph}}\left[\begin{array}{c} \bar{f}^1_{y_1y_2}\left(\bar{f}^1_{y_1y_1} + \bar{f}^1_{y_2y_2}\right) - \bar{f}^2_{y_1y_2}\left(\bar{f}^2_{y_1y_1} + \bar{f}^2_{y_2y_2}\right) \\ -\bar{f}^1_{y_1y_1}\bar{f}^2_{y_1y_1} + \bar{f}^1_{y_2y_2}\bar{f}^2_{y_2y_2} \end{array}\right] \tag{A12}$$

where for instance $\bar{f}^1_{y_1y_1y_1} = \left(\partial^3\bar{f}^1/\partial y_1^3\right)_{y_1=0}$ and so on. From Eqs (A5)-(A7), (A9) and (A11), the first Lyapunov value can be expressed as:

ACCEPTED MANUSCRIPT

$$L_1 = \frac{1}{16}\left(6a_{30}^1 + 2a_{12}^1 + 2a_{21}^2 + 6a_{03}^2\right) + \frac{1}{16\omega_{aph}}\left[\begin{array}{c} a_{11}^1\left(2a_{20}^1 + 2a_{02}^1\right) - a_{11}^2\left(2a_{20}^2 + 2a_{02}^2\right) \\ -4a_{20}^1 a_{20}^2 + 4a_{02}^1 a_{02}^2 \end{array}\right] \quad \text{(A13)}$$

b) Real and negative eigenvalues:

$$\lambda_{1,2} = \pm j\omega_{aph} \;;\; \lambda_3 = \alpha_1 \;;\; \lambda_4 = \alpha_2 \;;\; \alpha_{1,2} = -\xi/\tau \pm \sqrt{\xi^2 - (1 - f_k)}/\tau \quad \text{(A14)}$$

In this case, both α_1 and α_2 are negative since $\xi^2 > 1 - f_k$. The previously described steps can be applied but taking into account that now we have that:

$$y' = P_b \bar{y} \Rightarrow \begin{bmatrix} y_1' \\ y_2' \\ y_3' \\ y_4' \end{bmatrix} = \begin{bmatrix} 0 & 1 & 0 & 1 \\ \omega_{aph} & 0 & \alpha_1 & \alpha_2 \\ 0 & -\omega_{aph}^2 & \alpha_1^2 & \alpha_2^2 \\ n_1 & -K_{ps} & m_4 & m_5 \end{bmatrix} \begin{bmatrix} \bar{y}_1 \\ \bar{y}_2 \\ \bar{y}_3 \\ \bar{y}_4 \end{bmatrix} \begin{cases} m_4 = \dfrac{-K_{ps}}{\tau_i \alpha_1} - K_{ps} - \alpha_1 \tau_d K_{ps} \\ m_5 = \dfrac{-K_{ps}}{\tau_i \alpha_2} - K_{ps} - \alpha_2 \tau_d K_{ps} \end{cases} \quad \text{(A15)}$$

and the first Lyapunov value can be calculated by assuming the following changes:

$$\begin{array}{c} n_3 \to m_4 \;;\; m_3 \to m_5 \;;\; \omega_h \to \alpha_1 \\ \alpha \to \alpha_2 \;;\; n_2 \to \alpha_1^2 \;;\; m_2 \to \alpha_2^2 \end{array} \quad \text{(A16)}$$

References

[1] Khalil K., Nonlinear Systems, second ed., Prentice Hall, New Jersey, 1996.

[2] Ortega R., Loria A., Nicklasson P. J., Sira-Ramírez H., Passivity-based Control of Euler-Lagrange Systems, Springer-Verlag, London, 1998.

[3] Awrejcewicz J., Koruba Z., Classical Mechanics. Applied Mechanics and Mechatronics, Springer, New York, 2012.

[4] Arnold V. I., Lectures on bifurcations in versal families, Russ. Math. Surv. (1972) 54-123.

[5] Takens F., Forced oscillations and bifurcations, Comm. Math. Inst. Rijksuniv. Utrecht. 3 (1974) 1-59.

[6] Bogdanov R., Versal deformations of a singular point on the plane in the case of zero eigenvalues. Funct. Anal. Appl. 9 (1975) 144-145.

[7] Bogdanov R., Versal deformations of a singular point on the plane in the case of zero eigenvalues, Selecta Math. Soviet.1 (1981) 389-421.

[8] Carrillo F. A., Verduzco F., Control of a planar Takens-Bogdanov Bifurcation with Applications, Acta Appl. Math. 105 (2009) 199-255.

[9] Carrillo F. A., Verduzco F., Delgado J., Analysis of the Takens-Bogdanov bifurcation on m-parameterized vector fields, Int. J. Bifur. Chaos 20 (2010).

[10] Verduzco F., Carrillo F. A., Takens-Bogdanov Bifurcation Analysis in Indirect Field-oriented Control, AIP Conference Proceedings. 1368 (2011) 101-104

ACCEPTED MANUSCRIPT

[11] Hayato Chiba, Periodic orbits and chaos in fast–slow systems with Bogdanov Takens type fold points, J. Differential Equations. 250 (2011) 112-160.
[12] Polo M.F.P., Molina M.P., Stabilization and positioning control of a rolling disk by using the Bogdanov-Takens bifurcation, Physica D. 241 (2012) 1450-1469.
[13] Verduzco F., Alvarez J., Hopf bifurcation control: A new approach, Syst. Control Lett. 55 (2006) 437-451.
[14] Guckenheimer J., Holmes P., Nonlinear Oscillations, Dynamical Systems and Bifurcations of Vector Fields. Springer Verlag, New York, 1983.
[15] Kuznetsov Y.A., Elements of Applied Bifurcation Theory, third ed., Springer Verlag, New York, 1998.
[16] Wiggins S., Introduction to Applied Nonlinear Dynamical Systems and Chaos, second ed., Springer Verlag, New York, 2003.
[17] Pérez Polo Manuel F., Pérez Molina M., Regular self-oscillating and chaotic behaviour of a PID controlled gimbal suspension gyro. Chaos Soliton Fra. 21 (2004) 1057-1074.
[18] Verduzco F., Alvarez J., Hopf bifurcation control: a new approach, Systems and Control Lett. 55 (6) (2006) 437-451.
[19]. Pérez Polo Manuel F, Pérez. Molina M., A generalized mathematical model to analyze the nonlinear behavior of a controlled gyroscope in gimbals. Nonlinear Dynam, 48 (2007) 129-152.
[20] Perez-Molina Manuel, Perez-Polo Manuel F., Fold-Hopf bifurcation, steady state, self-oscillating and chaotic behavior in an electromechanical transducer with nonlinear control, Commun Nonlinear Sci Numer Simulat, 17 (2012) 5172-5188.
[21] Vidyasagar V., Nonlinear Systems, Pentice Hall, New York, 1994.
[22] Sastry S., Nonlinear Systems. Analysis, stability and control, Springer-Verlag, New York, 1999.
[23] Stane Kodba, Matjaž Perc, Marko Marhl. Detecting chaos from a time series, European Journal of Physics, 26, (2005) 205-215.
[24] Shilnikov L. P., Shilnikov A. L., Turaev D. V., Chua L. O., Methods of Qualitative Theory in Nonlinear Dynamics. Part II New Jersey, World Scientific, 2001.
[25] Glendinning P., Stability, instability and chaos: an introduction to the theory of nonlinear differential equations, New York, Cambridge University Press, 1996.
[26] Wagemakers Alexandre, Zambrano Samuel, Sanjuan Miguel A. F., Partial control of transient chaos in electronic circuits, International Journal Bifurcations and Chaos, 22 (2012) 1250032.
[27] Sabuco Juan, Sanjuan Miguel A. F., Yorke James A., Dynamics of partial control, Chaos, 22 (2012) 047507.
[28] Sabuco Juan, Zambrano Samuel, Sanjuan Miguel A. F., Yorke James A., Fiding safety in partially controllable chaotic systems, Commun Nonlinear Sci Numer Simulat, 17 (2012) 4274–4280.
[29] Starzhinskii V.M., Applied Methods in the Theory of Nonlinear oscillations. Mir Publishers, Moscow, 1980.
[30] Yamapi R., Dynamics of an electromechanical damping device with magnetic coupling,
[31] Chang Wei-Der, Shih Shun-Peng, PID controller design of nonlinear systems using an improved particle swarm optimization approach, Commun Nonlinear Sci Numer Simulat, 15 (2010) 3632–3639.
[32] Coelho Leandro dos Santos, Tuning of PID controller for an automatic regulator voltage system using chaotic optimization approach, Chaos Solitons Fra. 39 (2009) 1504-1514.

ACCEPTED MANUSCRIPT

[33] Polo M.F.P., Albertos P., Galiano J.A.B., Tuning of a PID controller gyro using the bifurcation theory, Syst. Control Lett. 57 (2008) 10-17.
[34] Lichtenberg A.J., Lieberman M.A., Regular and chaotic dynamics, second ed., Springer-Verlag, New York, 1992.
[35] Benettin G., Galgani L., Giorgilly A., Strelcyn J.M., Lyapunov characteristic exponents for smooth dynamical systems and for Hamiltonian systems: a method fro computing all of then, Part I: Theory, Meccanica 15(1980) 9-20.
[36] Benettin G., Galgani L., Giorgilly A., Strelcyn J.M., Lyapunov characteristic exponents for smooth dynamical systems and for Hamiltonian systems: a method fro computing all of then, Part II: Numerical applications, Meccanica 15(1980) 21-30.
[37] Pérez Manuel, Font Rafael, Montava Marco A., Regular self-oscillating and chaotic dynamics of a continuous stirred tank reactor, Comp. & Chem. Eng. 26 (2002) 889-901.
[38] Ott E., Gregobi C., Yorke J.A., Controlling Chaos, Phys. Rev. Lett., 64 (1990) 1196-1198.

ACCEPTED MANUSCRIPT

ACCEPTED MANUSCRIPT

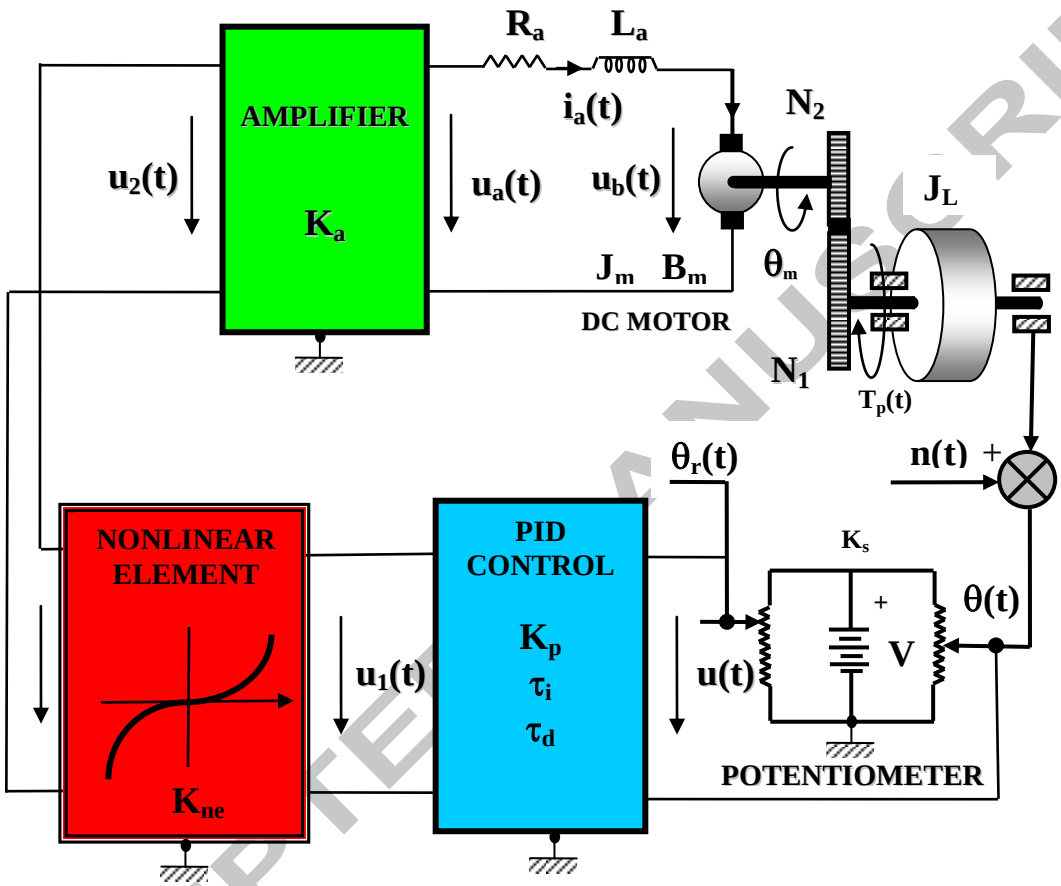

Figure 1

ACCEPTED MANUSCRIPT

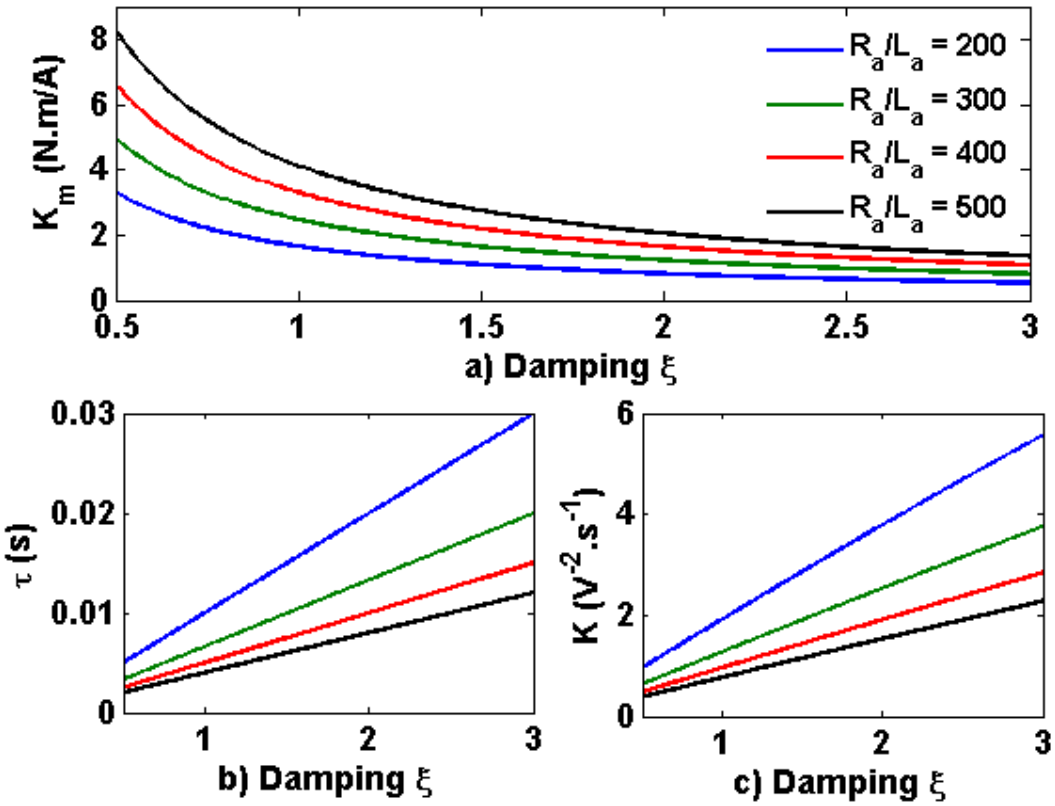

Figure 2

ACCEPTED MANUSCRIPT

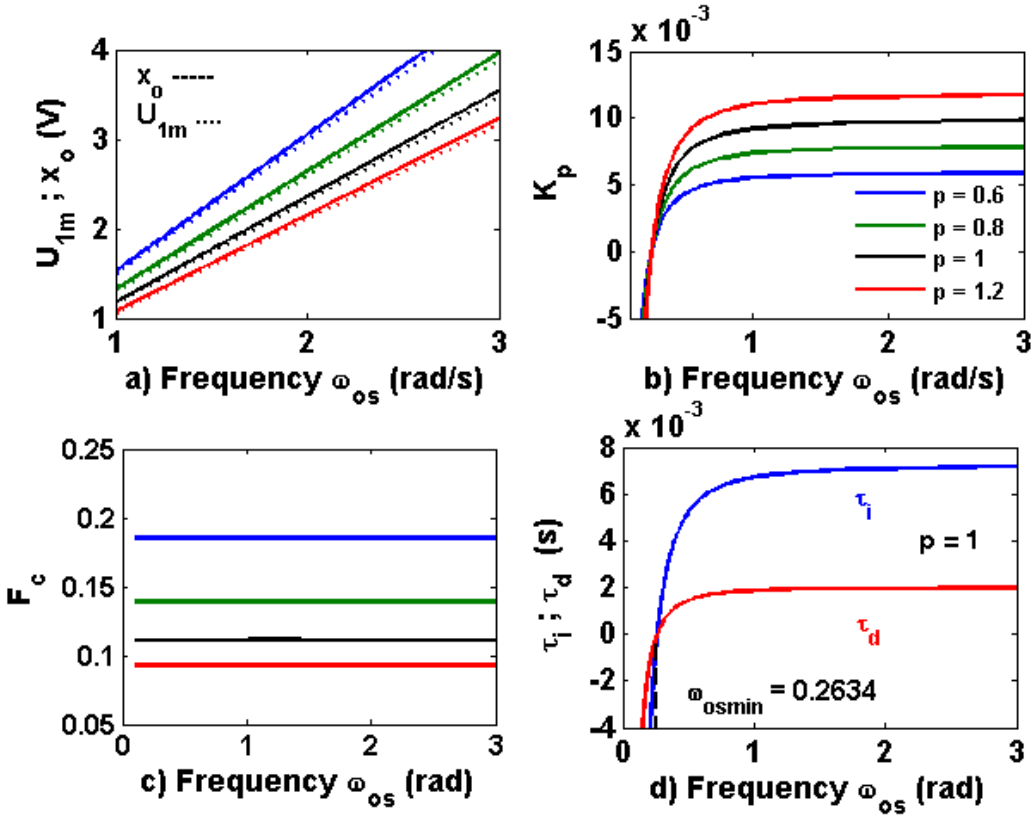

Figure 3

ACCEPTED MANUSCRIPT

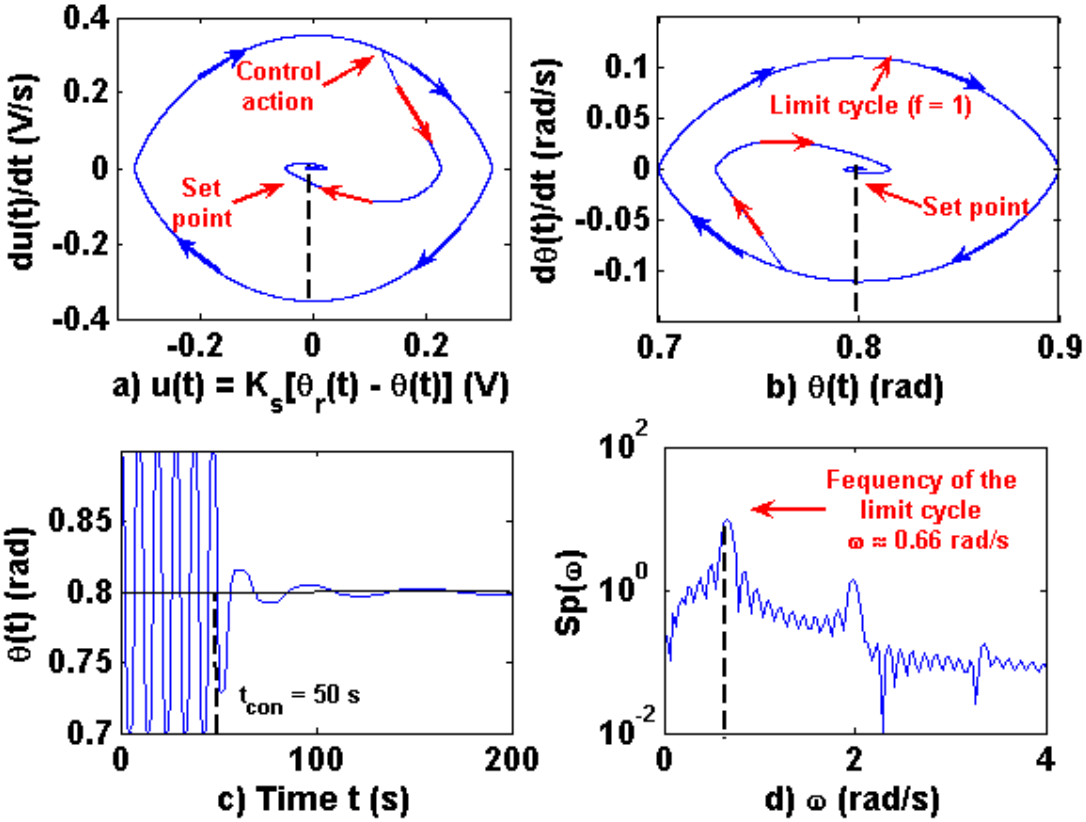

Figure 4

ACCEPTED MANUSCRIPT

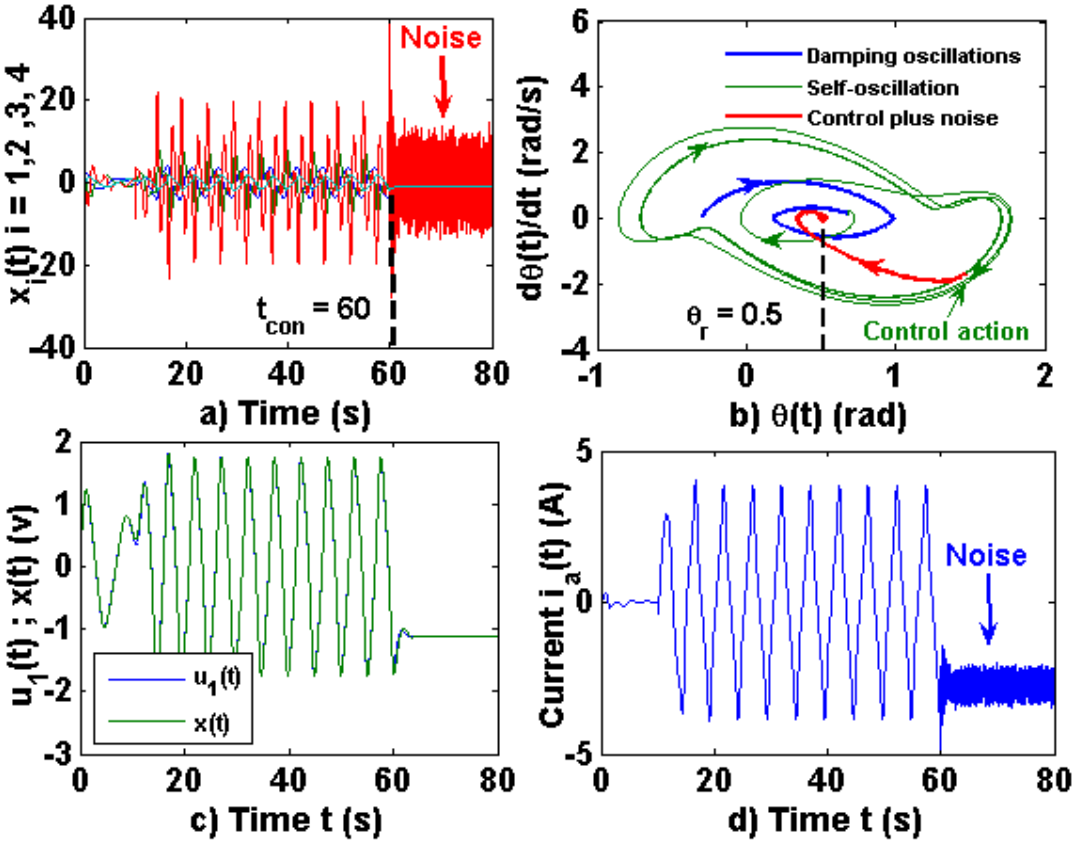

Figure 5

ACCEPTED MANUSCRIPT

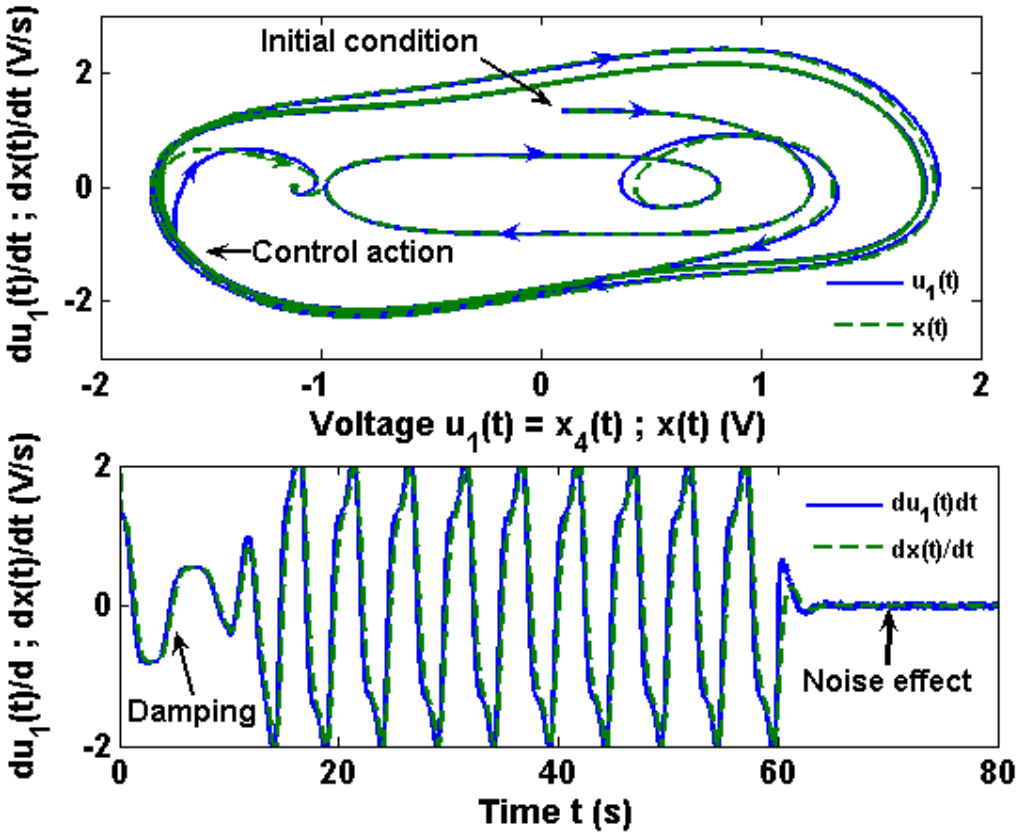

Figure 6

ACCEPTED MANUSCRIPT

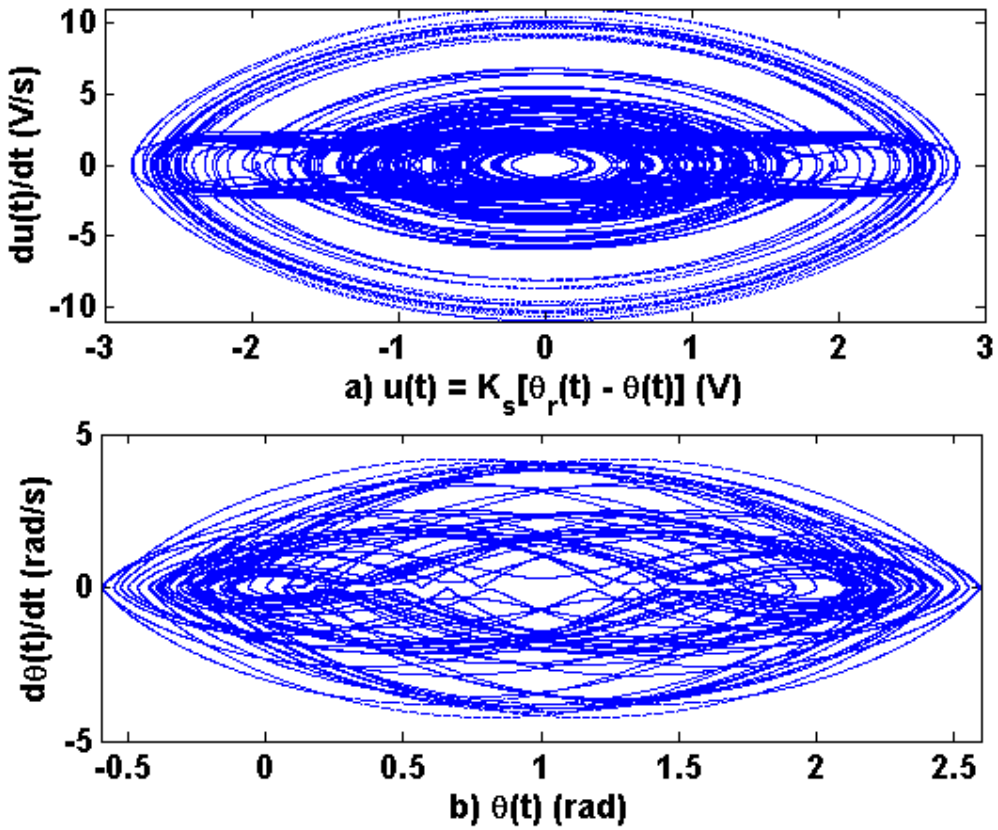

Figure 7

ACCEPTED MANUSCRIPT

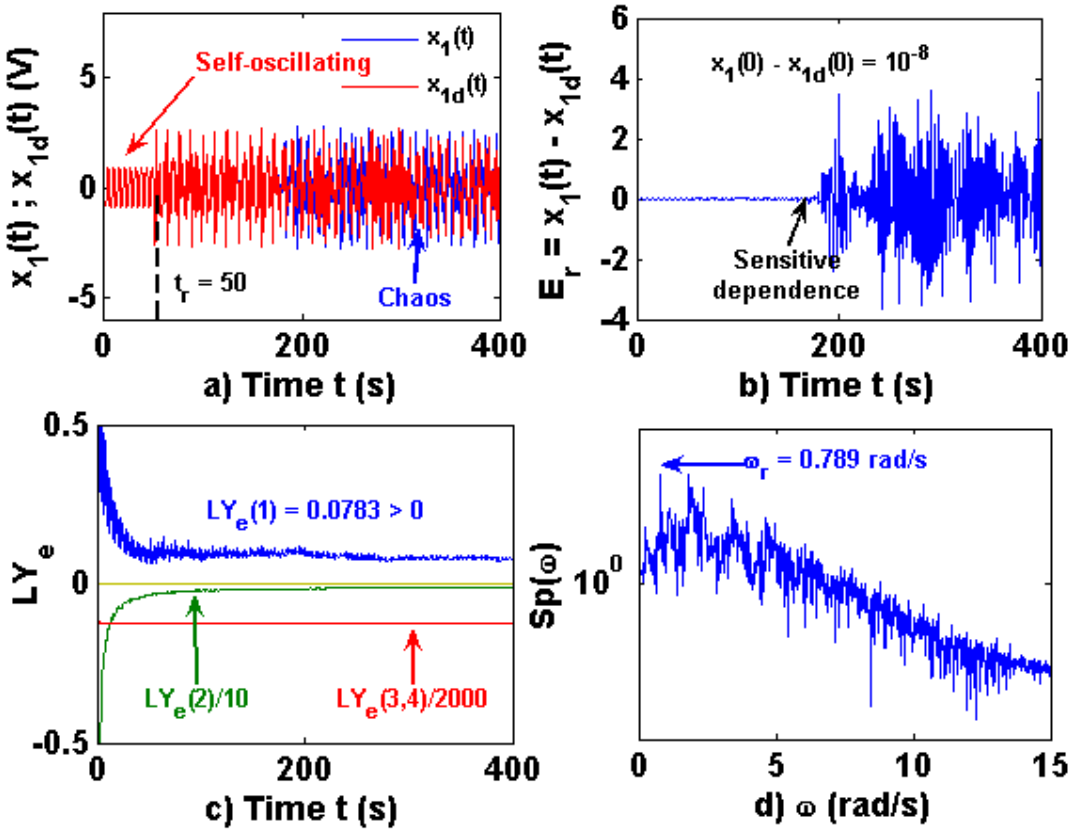

Figure 8

ACCEPTED MANUSCRIPT

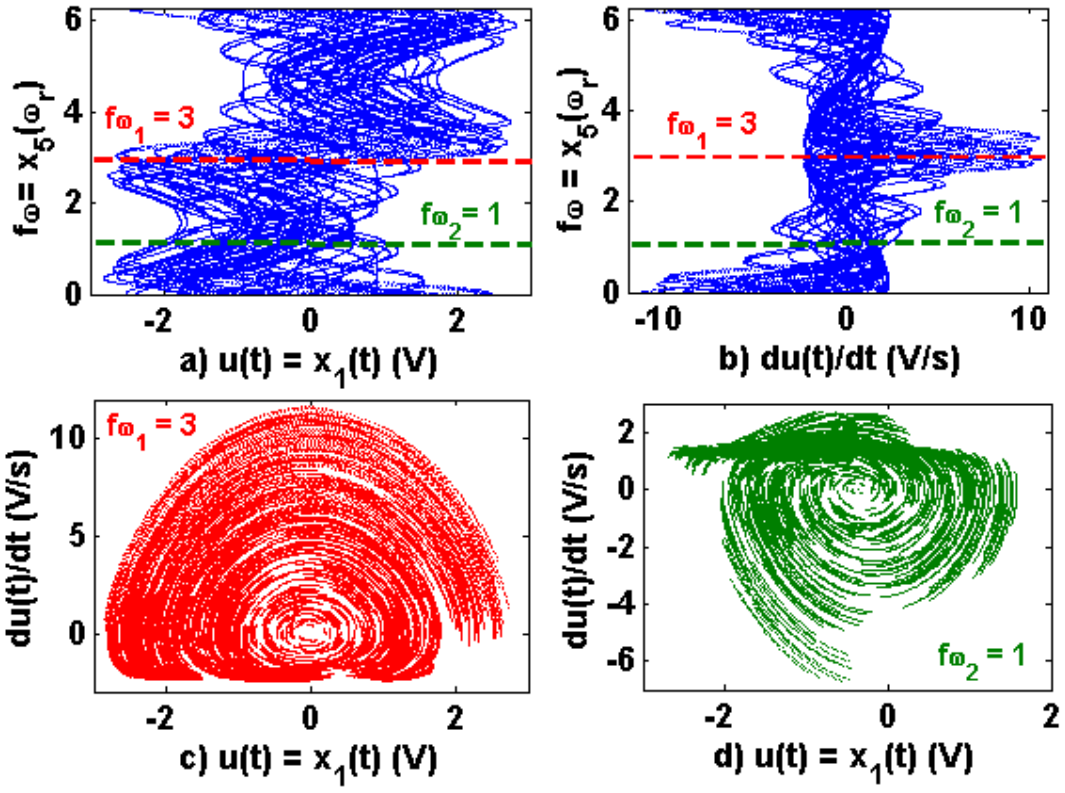

Figure 9

ACCEPTED MANUSCRIPT

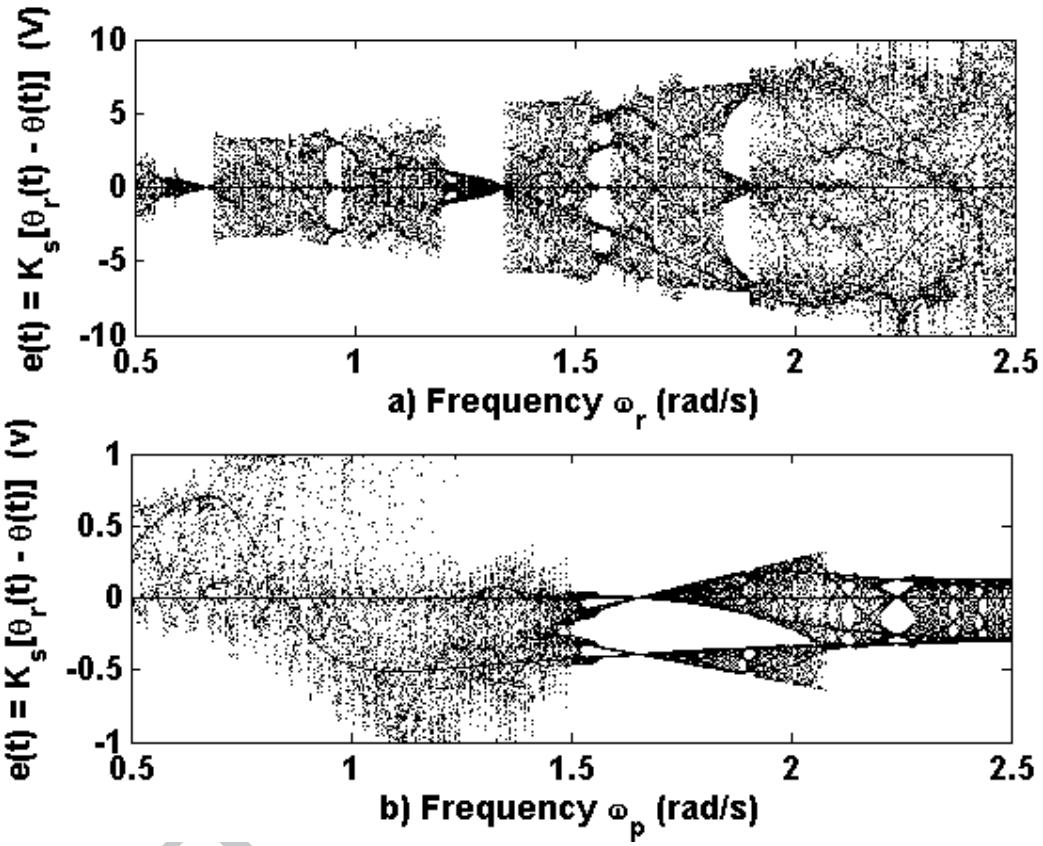

Figure 10

ACCEPTED MANUSCRIPT

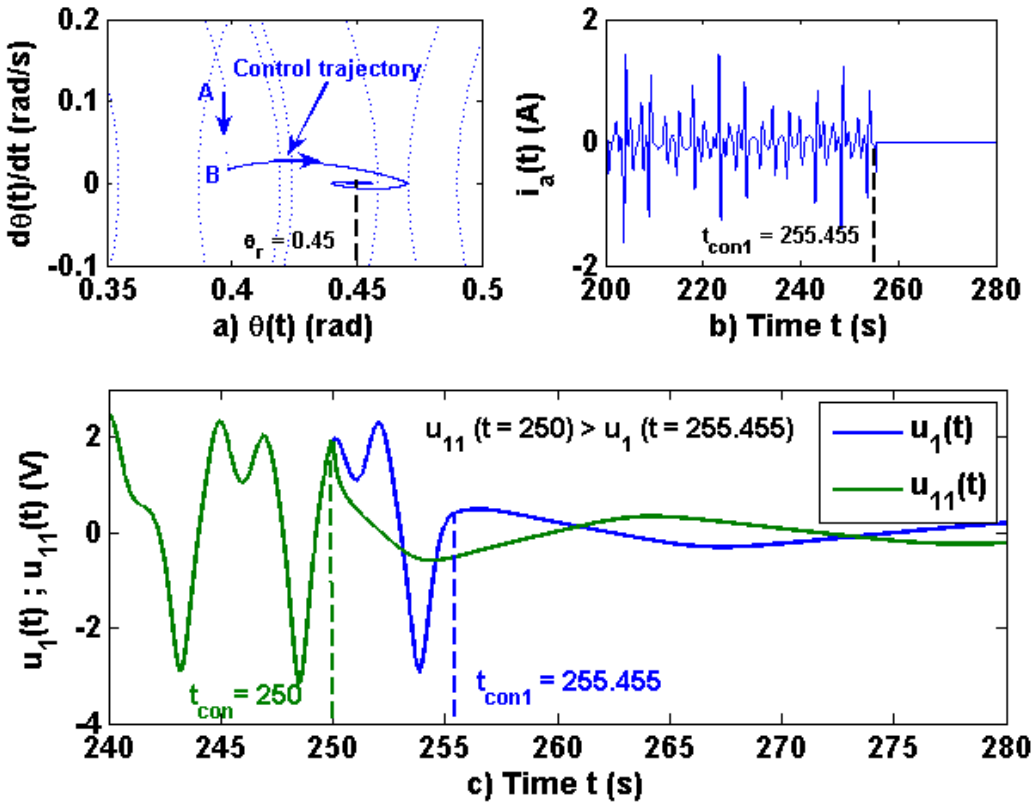

Figure 11

ACCEPTED MANUSCRIPT

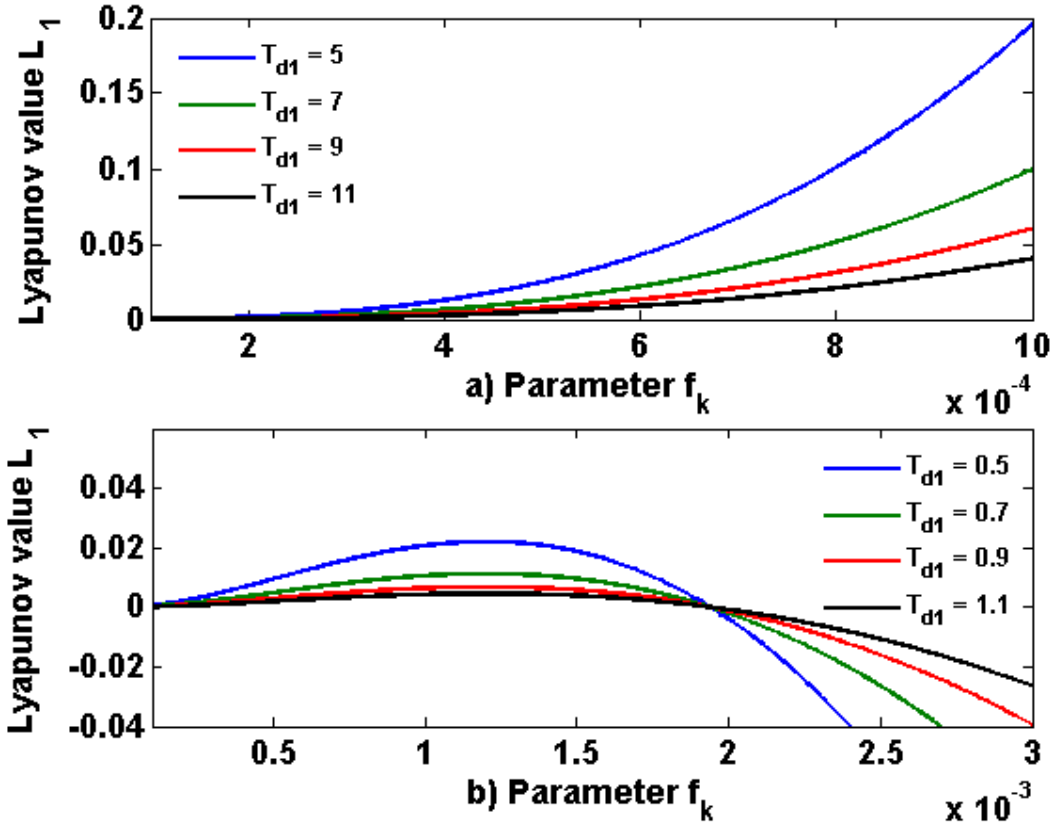

Figure 12

ACCEPTED MANUSCRIPT

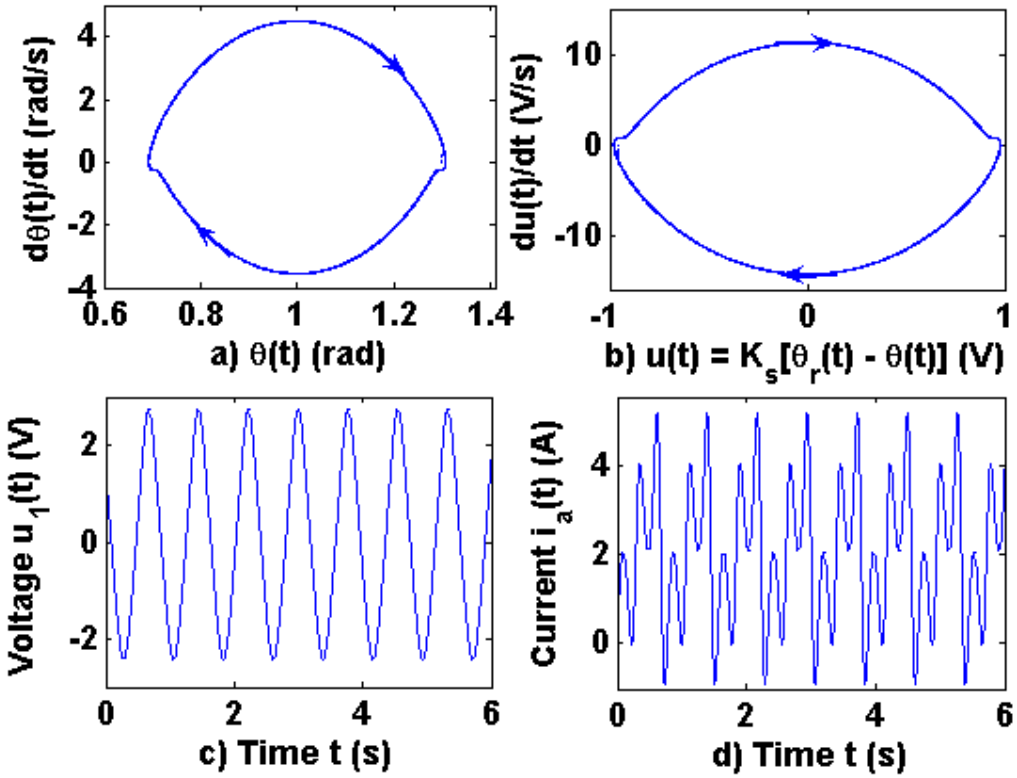

Figure 13

ACCEPTED MANUSCRIPT

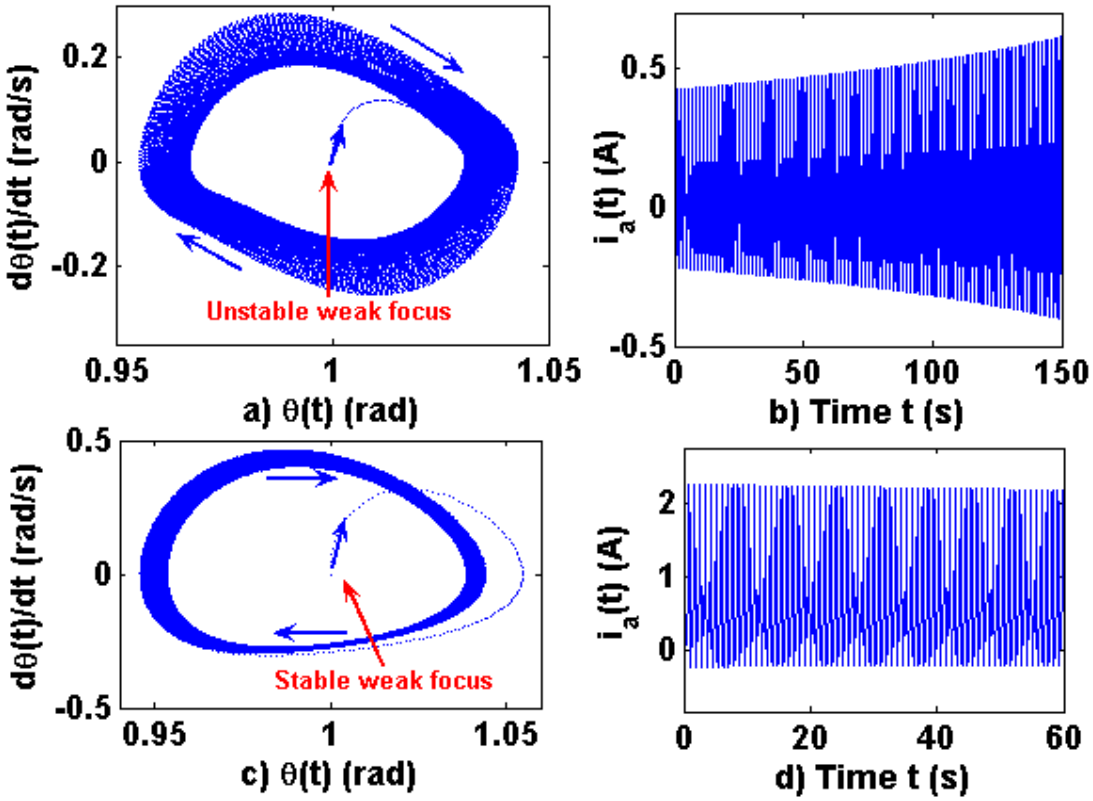

Figure 14

ACCEPTED MANUSCRIPT

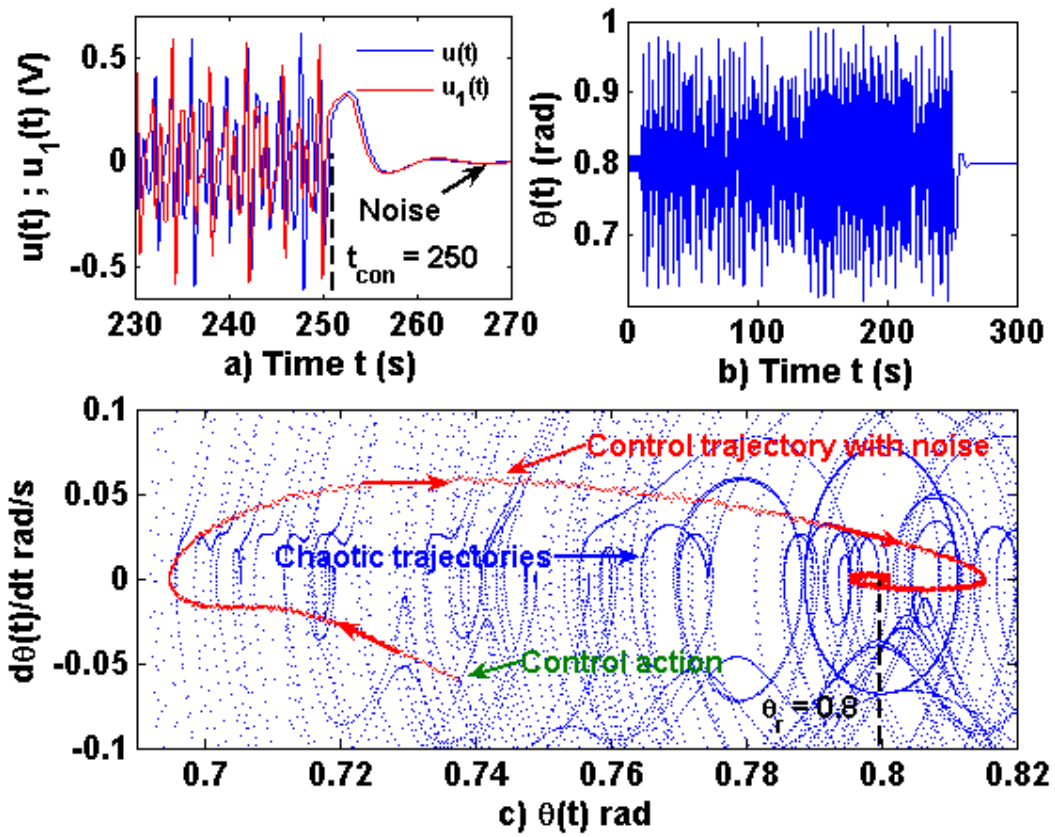

Figure 15

ACCEPTED MANUSCRIPT

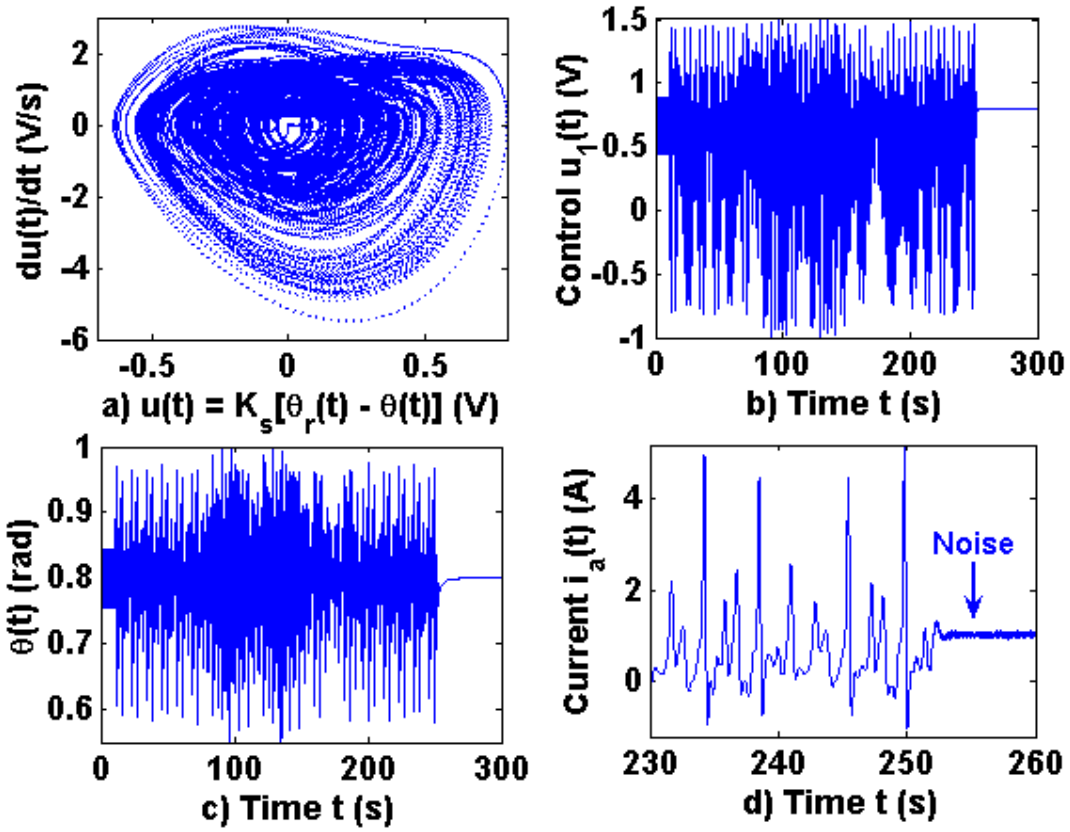

Figure 16

ACCEPTED MANUSCRIPT

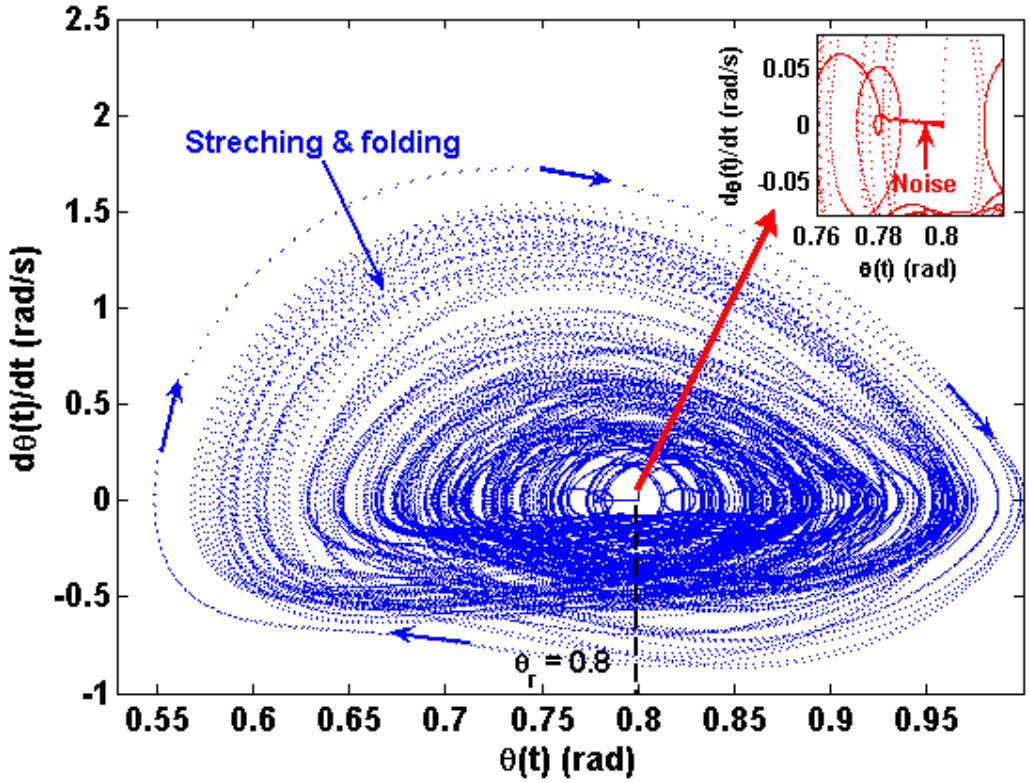

Figure 17

ACCEPTED MANUSCRIPT

TABLE 1. NOMINAL OPERATING CONDITIONS AND PARAMETER VALUES

Variable	Description	Value
K_a	Amplifier constant	100
R_a	Armature resistance (Ω)	5
L_a	Armature inductance (H)	0.01
J_m	Shaft motor moment of inertia (N.m.s^{-2})	$1.36.10^{-2}$
B_m	Viscous friction coefficient (N.m.s)	$9.64.10^{-3}$
J_L	Moment of inertia of the load (N.m.s^{-2})	1.36
B_L	Load viscous coefficient (N.m.s)	0.136
n	Gear train ratio (N_1/N_2)	1/10
K_m	Motor torque coefficient (N.m/A)	< 7
K_b	Back-electromotive force (V.s/rad)	= K_m
K_{ne}	Nonlinear element constant (V^{-2})	0.1
K_s	Potentiometer constant (V/rad)	$20/2\pi$
J_{me}	Equivalent moment of inertia (N.m.s^{-2})	$2.72.10^{-2}$
B_{me}	Equivalent viscous load (N.m.s)	$1.1.10^{-2}$
i_a	Armature current (A)	$-6 < i_a < 6$
u(t)	Imput voltage to PID controller (V)	
u_1	Control voltage (V)	$-10 < u_1 < 10$
ξ	Damping coefficient	$0.5 < \xi \leq 5$
τ	Time constant (s)	≥ 0.0038
K’	System parameter (V^{-1}.s^{-1})	0.23 to 3.14
K	System parameter K_mK_sK’ (V^{-2}.s^{-1})	0.72 to 10
K_p	Proportional constant of the PID controller	$10^{-3} < K_p < 2$
τ_i	Reset time of the PID controller (s)	$\tau_i \geq 7.10^{-3}$
τ_d	Derivative constant of the PID controller (s)	$\tau_d \geq 10^{-3}$
FC	Filter coefficient	≤ 0.1111
ω_{0s}	Self-oscillation frequency (rad/s)	$0.1 \leq \omega_{0s} \leq 9$
θ_{r1}	Constant set point (rad)	$-1 < \theta_{r1} < 1$
θ_{r2}	Amplitude of the set point (rad)	$-2 < \theta_{r2} < 2$
ω_r	Disturbance frequency (rad/s)	$1 < \omega_r < 5$
T_{d1}	Disturbance torque (N)	$0 \leq T_{d1} \leq 10$
T_{d2}	Amplitude of the disturbance torque (N)	$0 \leq T_{d2} \leq 5$
ω_d	Disturbance frequency (rad/s)	$1 < \omega_d < 5$
r_{ax}	Horizontal axis of the capture zone (rad)	≤ 0.3
r_{ay}	Vertical axis of the capture zone (rad/s)	≤ 0.2
p	Dimensional parameter (V^{-2}s^2)	1
f	Dimensionless parameter	$0.9 < f < 150$
L_1	First Lyapunov value	> 0, or < 0

ACCEPTED MANUSCRIPT

Figure captions

Figure 1. Schematic diagram of the controlled servomechanism with a reference input $\theta_r(t)$, an external disturbance torque $T_d(t)$ and a noise signal n(t). The feedback system is formed by a PID controller together with an amplifier with a constant K_a. The DC motor is controlled by field (the parameter values are indicated in table 1).

Figure 2. Parameter values obtained for L_a = 0.01 H. a) Values of the motor constant K_m, b) time constant τ and c) system constant K as a function of the damping coefficient ξ and R_a/L_a (Eqs (13)).

Figure 3. a) Variations of U_{1m} and x_0 as a function of the self-oscillation frequency for different values of p. b) Dependence of the proportional constant of the PID controller as a function of the self-oscillation frequency for different values of p. c) Filter coefficient F_c deduced from Eq (47) for different values of p. d) Reset time and derivative constant of the PID controller as a function of the self-oscillation frequency.

Figure 4. Simulation results obtained through the fourth-order Runge-Kutta method with the following parameter values in self-oscillating regime: Simulation time $t = 200$ s, simulation step $T = 0.005$ s, $K_a = 100$, $\xi = 0.95$, $\tau = 3.7969.10^{-3}$ s, $K_m = 4.3373$ $N.m/A$, $p = 1$, $f = 1 + 10^{-6}$, $\omega_{osmin} = 0.2634$ rad/s, $\omega_{os1} = 0.28$, $\omega_{os2} = 3$, $f_{1min} = 0.1153$, $f_{1max} = 0.9923$, $\omega_{os} = 0.65$ rad/s, $f_1 = 0.8358$, $K_p = 0.0099$, $\tau_i = 0.0072$ s, $\tau_d = 0.0017$ s, $U_{1m} = 0.7506$, $\theta_{r1} = \theta_{r2} = 0$ and $T_{d2} = 0$. The initial conditions are $x_o = [0\ 0\ 0\ 0.7506]$. The stability regime is applied at $t_{con} = 50$ s with $f = 200$, $K_{pc} = 1.9718$, $\tau_{ic} = 1.4428$ s and $\tau_{dc} = \tau_d = 0.0017$ s with a set point given by $\theta_{sp} = 0.8$ rad. a) Self-oscillating and steady state behavior in the phase plane e(t)-de(t)/dt. b) Self-oscillating and steady state behavior in the phase plane $\theta(t)$- $d\theta(t)/dt$. c) Time evolution of the angle of the device shaft. d) Power spectral density of the control signal $u_1(t)$.

Figure 5. Simulation results obtained through the fourth-order Runge-Kutta method with the following parameter values in the self-oscillation regime: Simulation time $t = 80$ s, simulation step $T = 0.004$ s, $K_a = 100$, $\xi = 2.5$, $\tau = 9.9919.10^{-3}$ s, $K_m = 1.6338$, $K = 1.9089$ $N.m/A$, $p = 1$, $f = 5$, $K_p = 0.1309$, $\tau_i = 0.2498$ s, $\tau_d = 0.004$ s,, $\theta_{r1} = 1$, $\theta_{r2} = 0$ and $T_{d1} = 0$, $T_{d2} = 4.567$ N, $\omega_d = 1.234$ rad/s. The initial conditions are $x_0 = [2.5455\ 0\ 0\ 0.1]$. The stability regime is applied at $t_{con} = 60$ s with $f = 10$ and the new control PID parameters are $K_{pc} = 0.2617$, $\tau_{ic} = 0.4996$ s and $\tau_{dc} = \tau_d = 0.004$ s with a set point given by $\theta_{sp} = 0.5$ rad. a) State variables as a function of the time. b) Limit cycle of the system given by Eqs (15). c) Variables $u_1(t)$ and $x(t)$ as a function of the time. d) Armature current as a function of the time.

Figure 6. Phase portrait of $u_1(t)$-$du_1(t)/dt$ and $\bar{x}(t) - \bar{y}(t)$. b) Value of $du_1(t)/dt$ deduced from the variables $x_4(t)$ and $\bar{y}(t) = d\bar{x}(t)/dt$ as a function of the time (simulation values are indicated in the legend of Fig 5).

ACCEPTED MANUSCRIPT

Figure 7. a) Strange attractor in the phase plane u(t)-du(t)/dt. b) Strange attractor in the phase plane θ(t)-dθ(t)/dt. Simulation results obtained through the fourth-order Runge-Kutta method with the following parameter values in the self-oscillation regime: K_a = *100,* ξ *= 0.95, p = 1, f = 1+* 10^{-6}, f_1 *= 0.9827,* K_p *= 0.0099,* τ_i *= 0.0072 s,* τ_d *= 0.002 s,* U_{1m} *= 2.3094 V,* x_0 *= 2.3607 V,* F_c *= 0.1111,* simulation time *t = 400 s,* simulation step *T = 0.002 s,* self-oscillation frequency ω_{os} *= 0.9 rad/s* and initial conditions x_0 *= [-0.6996 0 0 1.0623 0 0*]. At *t* = t_r it holds that $T_{d1} = T_{d2} = 0$, θ_{r1} *= 1 rad,* θ_{r2} *= 0.987 rad* and ω_r *= 0.789 rad/s.*

Figure 8. a) Self-oscillating and chaotic behavior with sensitive dependence of the input voltage of the PID controller $x_1(t) \equiv u(t)$. b) The difference between $x_1(t)$ and u(t) allows to appreciate the sensitive dependence with two initial conditions that are very close. c) All Lyapunov exponents as a function of the time, being one of them positive. d) The peak of the power spectral density of $x_1(t) \equiv u(t)$ allows to identify the external applied frequency (the simulation and parameters values are indicated at the legend of Fig 7).

Figure 9. Simulation results obtained through the fourth-order Runge-Kutta method taking a simulation time of 10000 s and a simulation step of 0.002 s (the rest of parameter values are indicated at legend of Fig 7). a) Angular variable f_ω ($0 < f_\omega < 2\pi$) associated to the external disturbance and external frequency ω_r as a function of the voltage u(t). b) Angular variable $x_5 \equiv f_\omega$ ($0 < f_\omega < 2\pi$) associated to the external disturbance and external frequency ω_r as a function of du(t)/dt. c) Poincaré section obtained for the values of $f_{\omega 1}$ and $f_{\omega 2}$ indicated in a) and b). d) Poincaré section obtained for the values of $f_{\omega 1}$ and $f_{\omega 2}$ indicated in a) and b).

Figure 10. a) Bifurcation diagram obtained through the calculation of the Poincaré sections for the system defined by Eqs (15) (see Figs 9 c) and d)) with K_a *= 100,* ξ *= 0.95, p = 1, f = 1,* K_p *= 0.0099,* τ_i *= 0.0072 s,* τ_d *= 0.002 s,* simulation time *t = 400 s,* simulation step *T = 0.002 s* and initial conditions x_0 *= [0 0 0 0.5902 0 0*]. At *t* = t_r it holds that $T_{d1} = T_{d2} = 0$, θ_{r1} *= 0 rad* and θ_{r2} *= 1.234 rad.* b) Same as figure 10 a) but taking K_a *= 100,* ξ *= 0.95, p = 1, f = 1,* K_p *= 0.0099,* τ_i *= 0.0072 s,* τ_d *= 0.002 s,* simulation time *t = 400 s,* simulation step *T = 0.002 s* and initial conditions x_0 *= [0 0 0 0.5902 0 0*]. At *t* = t_r it holds that $T_{d1} = 0$, $T_{d2} = 2.55$ and $\theta_{r1} = \theta_{r2} = 0$.

Figure 11. Simulation results obtained through the fourth-order Runge-Kutta method with the following parameter values in the self-oscillating regime: K_a *= 100,* ξ *= 0.95, p = 1, f = 1,* K_p *= 0.0099,* τ_i *= 0.0072 s,* τ_d *= 0.0019 s,* simulation time *t = 400 s,* simulation step *T = 0.005 s* and initial conditions x_0 *= [0 0 0 0.5902 0 0*]. At *t* = t_{con} *= 250s* the capture region is $\Omega(r_{ax} = 0.5, r_{ay} = 0.4)$ whereas *f =150,* K_{pc} *= 1.4788,* τ_{ic} *= 1.0821 s,* τ_{dc} *= 0.0019 s,* $T_{d1} = T_{d2} = 0$, $\theta_{r1} = 0$, θ_{r2} *= 1.234 rad* and ω_r *= 1.125 rad/s.* a) Phase plane θ(t)-dθ(t)/dt showing that points A and B are inside the capture zone. b) Armature current. c) Control signals $u_1(t)$ and $u_{11}(t)$.

Figure 12. First Lyapunov value plotted as a function of the parameter f_k. a) ξ = 0.95, for which the eigenvalues are $\lambda_{1,2} = \pm j\omega_{aph}$ and $\lambda_{3,4} = -250.02 \pm j82.19$. b) ξ = 5, for

ACCEPTED MANUSCRIPT

which the eigenvalues are $\lambda_{1,2} = \pm j\omega_{aph}$, $\lambda_3 = -495.35$ and $\lambda_4 = -5.055$. In both cases it has been assumed that $f_d = 0.8$.

Figure 13. Self-oscillating behavior caused by an APH bifurcation. Simulation results obtained through the fourth-order Runge-Kutta method with the following parameter values in the self-oscillating regime: $K_a = 100$, $\xi = 0.95$, $p = 1$, $f = 1$, $K_p = 0.13345$, $\tau_i = 7.215.10^{-3}$ *s*, $\tau_d = 1.5987.10^{-3}$ *s*, simulation time $t = 40$ *s*, simulation step $T = 0.005$ *s*, initial conditions $x_0 = [-0.9549\ 0\ 0\ 0.5\ 0\ 0]$ and self-oscillation frequency $\omega_{aph} = 6.4512$ rad/s. The eigenvalues associated to the weak focus are $\lambda_{1,2} = \pm j6.4512$ and $\lambda_{3,4} = -250.02 \pm j82.187$, and at the equilibrium point we have that $y_{4e} = 1.0124$ *V*, $T_{d1} = 0.9$ *N.m*, $T_{d2} = 0$, $\theta_{r1} = 1$ *rad*, $\theta_{r2} = 0$, first Lyapunov value $L_1 = 1.0881.10^{-4}$ and $f_k = 1.2.10^{-4}$. a) Limit cycle in the phase plane $\theta(t)$-$d\theta(t)/dt$. b) Limit cycle in the phase plane $u(t)$-$du(t)/dt$. c) Control signal. d) Armature current $i_a(t)$.

Figure 14. Unstable and stable weak focus plotted in the phase plane $\theta(t)$-$d\theta(t)/dt$. The simulation results have been obtained for $K_a = 100$, $\xi = 5$, $p = 1$, $f = 1$, a simulation time $t = 200$ *s*, a simulation step $T = 0.005$ *s* and initial conditions $x_0 = [1\ 0\ 0\ 0.4\ 0\ 0]$. a) Unstable weak focus for $T_{d1} = 0.03$ *N*, $f_k = 1.2.10^{-3}$, $L_1 = 12.6337 > 0$, $K_p = 3.0867$, $\tau_i = 0.2001$ *s*, $\tau_d = 1.5987.10^{-3}$ *s* and $\omega_{aph} = 3.8761$ *rad/s*. b) Armature current with an unstable weak focus. c) Stable weak focus for $T_{d1} = 0.51$ *N*, $f_k = 6.10^{-3}$, $L_1 = -1.2092 < 0$, $K_p = 2.8788$, $\tau_i = 0.2010$ *s*, $\tau_d = 1.5987.10^{-3}$ *s* and $\omega_{aph} = 8.6673$ *rad/s*. d) Armature current with a stable weak focus.

Figure 15. Simulation results obtained through the fourth-order Runge-Kutta method with $K_a = 100$, $\xi = 0.95$, $p = 1$, $T_{d1}=9$ *N.m*, $f_k = 1.2.10^{-4}$, $\omega_{aph} = 6.4512$ *rad/s*, $\lambda_{1,2} = \pm j6.4512$, $\lambda_{3,4} = -250.02 \pm j82.187$ and $L_1 = 1.0881.10^{-4}$. The PID parameters before the control action are $K_p = 1.3345.10^{-1}$, $\tau_i = 7.215.10^{-3}$ *s* and $\tau_d = 1.5987.10^{-3}$ *s*, while the simulation time is $t = 300$ *s*, the simulation step is $T = 0.005$ *s*, and the initial conditions are $x_0 = [0\ 0\ 0\ 0.1\ 0\ 0]$. At $t = t_{con} = 250s$ we define a capture region $\Omega(r_{ax} = 0.3, r_{ay} = 0.2)$ with a seek time of 0.98 *s*, $f = 150$ and $f_{na} = 0.1$. The PID parameters after the control action at $t = 250.98$ *s* are $K_{pc} = 1.4788$, $\tau_{ic} = 1.0821$ *s*, $\tau_{dc} = 0.0016$ *s*, $T_{d2} = 10$ *N.m*, $\omega_p = 3.2256$ *rad/s*, $\theta_{r1} = 1$, $\theta_{r2} = 0$ and $\omega_r = 0$. a) Sensitive dependence of voltages $u(t)$ and $u_1(t)$, which differ in 10^{-8} at $t = 0$. b) Position of the motor shaft. c) Chaotic trajectories and control trajectory in the phase plane $\theta(t)$-$d\theta(t)/dt$ after the control action.

Figure 16. Simulation results obtained through the fourth-order Runge-Kutta method with $K_a = 100$, $\xi = 5$, $p = 1$, $T_{d1}= 0.52$ *N.m*, $f_k = 2.5.10^{-4}$, $\omega_{aph} = 5.5947$ *rad/s*, $\lambda_{1,2} = \pm j5.5947$, $\lambda_{3,4} = -495.3493, -5.0551$ and $L_1 = -0.049$. The PID parameters before the control action are $K_p = 1.1841$, $\tau_i = 0.2003$ *s* and $\tau_d = 0.0016$ *s*, while the simulation time is $t = 350$ *s*, the simulation step is $T = 0.005$ *s* and the initial conditions are $x_0 = [0\ 0\ 0\ 0.2\ 0\ 0]$. At $t = t_{con} = 250s$, we define a capture region $\Omega(r_{ax} = 0.3, r_{ay} = 0.2)$ with a seek time of 1.81 *s*, $f = 20$ and $f_{na} = 0.015$. The PID parameters after the control action at $t = 251.81$ *s* are $K_{pc} = 1.0808$, $\tau_{ic} = 3.9968$ *s*, $\tau_{dc} = 0.0016$ *s*, $T_{d2} = 0.45$ *N.m*, $\omega_p = 2.7973$ *rad/s*, $\theta_{r1} = 1$, $\theta_{r2} = 0$ and $\omega_r = 0$. a) Strange attractor in the phase plane u(t)-du(t)/dt. b) Control signal. c) Axis position of the motor shaft. d) Armature current (note the presence of noise after the control application).

ACCEPTED MANUSCRIPT

Figure 17. Strange attractor in the phase plane $\theta(t)$-$d\theta(t)/dt$, where the set point has been reached even in the presence of noise (parameter values are indicated in the legend of Fig 16).

ACCEPTED MANUSCRIPT

ACCEPTED MANUSCRIPT

Highlights

- Comparative analysis of Bogdanov-Takens and Andronov-Poincare-Hopf bifurcations.
- Tuning a PID controller using Bogdanov-Takens bifurcation and describing function.
- Tuning a PID controller by using the Andronov-Poincaré-Hopf bifurcation.
- Analysis of self-oscillating and chaotic behavior for the servomechanism.
- Use of chaotic behavior to improve the PID controller performance.

ACCEPTED MANUSCRIPT